Precambrian Research 314 (2018) 353–376

Contents lists available at ScienceDirect

Precambrian Research

journal homepage: www.elsevier.com/locate/precamres

Neoarchean reworking of TTG-like crust in the southernmost portion of the São Francisco Craton: U-Pb zircon dating and geochemical evidence from the São Tiago Batholith

Maurício Bulhões Simon[a], Everton Marques Bongiolo[b,*], Ciro Alexandre Ávila[c], Elson Paiva Oliveira[d], Wilson Teixeira[e], Rômulo Campos Stohler[f], Filipe Vidal Soares de Oliveira[g]

[a] Programa de Pós-graduação em Geologia (PPGL), Instituto de Geociências, Universidade Federal do Rio de Janeiro, Rio de Janeiro, RJ, Brazil
[b] Instituto de Geociências, Universidade Federal do Rio de Janeiro, Rio de Janeiro, RJ, Brazil
[c] Museu Nacional, Universidade Federal do Rio de Janeiro, Rio de Janeiro, RJ, Brazil
[d] Department of Geology and Natural Resources, Institute of Geosciences, University of Campinas – UNICAMP, Campinas, SP, Brazil
[e] Instituto de Geociências, Universidade de São Paulo, São Paulo, SP, Brazil
[f] Petrobras, UO-RIO/ATP-RO/RES, Rio de Janeiro, RJ, Brazil
[g] Petrobras, E&P-EXP/AFOE/ADGP, Rio de Janeiro, RJ, Brazil

A B S T R A C T

Field, petrographic and geochemical data combined with in situ zircon U-Pb LA-ICP-MS ages are documented for the São Tiago Batholith (southernmost portion of the São Francisco Craton) to understand its origin and magmatic evolution. The geologic relations indicate that the batholith is composed of granitic to granodioritic orthogneisses (L2) with tonalitic xenoliths (L1) intruded by pegmatite (L3) and metagranite (L4). L1 consists of two facies of tonalitic orthogneiss, one biotite-rich, and the other biotite-poor. The geochemical evidence, including high K_2O with mantle-like chemical signature, suggests that the Bt-rich tonalitic gneiss (2816 ± 30 Ma) was derived from contamination of mafic magmas by crustal-derived components. The Bt-poor tonalitic gneiss, of TTG affinity, was generated by partial melting of LILE-enriched mafic rocks, possibly from oceanic plateus in a subduction environment. L2 includes two distinct types of rocks: (i) granodioritic orthogneiss, chemically ranging from medium-pressure TTGs to potassic granitoids originated via partial melting of previous TTG crust, including L1 Bt-poor; and (ii) granitic gneiss (2664 ± 4 Ma), geochemically similar to crustal-derived granites, produced by melting of the L1 Bt-rich tonalitic gneiss or mixed TTG/metasedimentary sources. L3 pegmatite (2657 ± 23 Ma) results from melting of L2, whereas L4 metagranite (dikes and stocks) shows petrogenesis similar to that of the L2 granitic gneiss. Related orthogneisses occur near the São Tiago Batholith: (i) a hornblende-bearing tonalitic gneiss, and (ii) a hybrid hornblende-bearing granitic gneiss (2614 ± 13 Ma), whose genesis is linked with interaction of sanukitoid and felsic potassic melts, representing the last Archean magmatic pulse of the region. The Minas strata along the Jeceaba-Bom Sucesso lineament near our study region encircle the São Tiago Archean crust, representing an irregular paleo-coastline or a micro-terrane amalgamation with the São Francisco Proto-craton, with possible subsequent dome-and-keel deformational processes. Our petrological and geochronological data reevaluate nebulous concepts in the literature about the SFC, revealing (i) a chemically and compositionally diverse crustal segment generated at the Late Archean in diverse geodynamic scenarios, and (ii) a more complex lineament than previously thought in terms of the paleogeography of the southern São Francisco Craton.

1. Introduction

The evolution of Archean cratons is mostly marked by the formation of gray gneisses and greenstone belts. Economic interest in greenstone belts, hosts of Au and Ni mineralization, provided the basic geological knowledge of cratonic areas, which was followed by initial geochemical and geochronological studies on gray gneisses (Anhaeusser et al., 1969; Barker, 1979; Condie and Hunter, 1976; Heimlich and Banks, 1968). However, even with extensive compilations of field and geochronological data worldwide, many uncertainties remain concerning the

* Corresponding author.
E-mail address: ebongiolo@geologia.ufrj.br (E. Marques Bongiolo).

https://doi.org/10.1016/j.precamres.2018.06.015
Received 9 June 2017; Received in revised form 12 December 2017; Accepted 22 June 2018
Available online 28 June 2018
0301-9268/

geotectonic setting in which these gneisses formed, their petrogenesis and ages. This is particularly true for the São Francisco Craton in South America.

Moyen and Martin (2012) summarized the knowledge of gray gneisses and proposed their subdivision into a *plutonic component* that involves sodic and potassic granitoids and a *non-granitoid* portion. In this regard, tonalite-trondhjemite-granodiorite suites (TTGs) are the most important components of the sodic plutonic bodies, which widely prevailed during the formation of the Archean continental crust. Traditionally, most authors have proposed that TTGs were generated by differentiation of a basaltic parent, either by partial melting (Barker and Arth, 1976; Ellam and Hawkesworth, 1988; Martin, 1986) or fractional crystallization (Arth et al., 1978; Barker, 1979; Smith et al., 1983). Still, Moyen and Martin (2012) emphasized that the second process contradicts most of the observations, particularly due to the absence of any mafic and intermediate phases in TTG suites and the requirement of an excessively high degree of fractional crystallization.

A marked change in the lithological constitution of the Earth occurred during the end of the Archean and the Archean-Paleoproterozoic transition, represented by the waning or ending of TTG generation and profusion of K-rich granitoid formation (Frost et al., 2006; Moyen and Martin, 2012; Moyen et al., 2003; Sylvester, 1994). Laurent et al. (2014) suggested that the chronology of Late Archean granitoid emplacement varies from craton to craton but can generally be represented by a two-stage evolution: a long period of TTG emplacement followed by a relatively shorter period when biotite and two-mica granites, sanukitoids, and hybrid granitoids largely prevailed. Biotite and two-mica granites consist of crustal-derived granites that are widespread in every Archean craton (Feng and Kerrich, 1992; Moyen et al., 2003; Windley, 1995). They are high-silica peraluminous rocks with low ferromagnesian oxides and potassic signature, whose genesis is commonly associated with partial melting of older felsic crust, especially TTGs, and an eventual metasedimentary melting contribution (Almeida et al., 2013; Breaks and Moore, 1992; Moyen et al., 2003; Sylvester, 1994). The sanukitoid series and the hybrid granitoids generally constitute minor groups among the Late Archean granitoids in most cratons (Heilimo et al., 2010; Laurent et al., 2014). The contradictory geochemistry of the sanukitoids (enrichment in compatible Mg, Ni, and Cr and in incompatible LILE and LREE) is genetically linked with melting of a metasomatized mantle (Heilimo et al., 2010). The sanukitoid magmatism marks a change during the Late Archean in the main melting source of juvenile continental crust, from basalt to metasomatized mantle peridotite (Martin et al., 2009) and evidences the onset of “modern style” plate tectonics (Laurent et al., 2014). The term “hybrid granitoid” (Laurent et al., 2014) refers to Archean granitoids identified in many cratons (Almeida et al., 2013; Champion and Sheraton, 1997; Jayananda et al., 2006; Whalen et al., 2004) that formed through interaction between magmas or sources of any of the other three noted groups.

The southern São Francisco Craton includes several Paleo- to Neoarchean metamorphic complexes, but many areas lack detailed geochemical and geochronological studies. Most of the regional investigations in these complexes focused on the tectonic evolution and geochronology of the magmatic events that originally formed the TTGs and K-rich granitoids in the Quadrilátero Ferrífero region (Albert et al., 2016; Farina et al., 2015, 2016; Lana et al., 2013; Machado et al., 1992; Romano et al., 2013; Teixeira et al., 2017). However, few studies drew attention to the gneiss complexes southwest of the Quadrilátero Ferrífero (Campos et al., 2003; Teixeira et al., 1998), which are bounded to the south by the NE-trending Jeceaba-Bom Sucesso lineament. This lineament has been considered as the suture zone between the aforementioned Archean domains to the north and the Paleoproterozoic rocks of the Mineiro belt to the south (Campos et al., 2003; Campos and Carneiro, 2008).

Controversial geochronological data have been reported for the São Tiago Batholith, focus of this paper, which is peculiarly located to the south of the Jeceaba-Bom Sucesso lineament and approximately 80 km away from the Quadrilátero Ferrífero region. For instance, Silva et al. (2002) obtained a Paleoproterozoic SHRIMP U-Pb age in zircon of 2050 ± 12 Ma for a hornblende-bearing granodiorite near the town of São Tiago, whereas Toledo et al. (2010) reported Archean U-Pb (SHRIMP) zircon ages of 2701 ± 38 Ma for the paleosome and 2667 ± 43 Ma for the neosome in a single outcrop of the São Tiago Batholith.

This paper presents petrographic, geochemical and U-Pb LA-ICP-MS data on metagranitoids and gneisses that crop out near the São Tiago region, supported by detailed geological mapping at the 1:25,000 scale. Our work revealed a chemically and compositionally varied crustal segment formed at the Late Archean in diverse geodynamic settings. We have reexamined controversial and currently accepted concepts in the literature on the southern São Francisco Craton, providing more information about the present geotectonic framework of the craton, and a new understanding on the Jeceaba-Bom Sucesso lineament, previously thought to be linear and simple. Finally we present here insights on the paleogeography of the southern portion of the craton during the Archean-Paleoproterozoic transition.

2. Geotectonic framework of the southern São Francisco craton

The geotectonic framework of the southern São Francisco Craton comprises mostly Archean domains representative of the São Francisco Proto-craton, foreland of the south-bounding Mineiro belt, a Paleoproterozoic accretionary terrain (Fig. 1; Teixeira et al., 2017; Alkmim and Teixeira, 2017). The Neoproterozoic to Early Ordovician marginal belts associated with the assembly of Gondwana outline the final configuration of the craton to the west-southwest, southeast, and east (Fig. 1; Campos Neto et al., 2011; Trouw et al., 2013).

2.1. São Francisco Proto-craton

The southern portion of the São Francisco Proto-craton is mainly represented by dome-shaped metamorphic complexes, including gray gneisses, and the Rio das Velhas greenstone belt, both Meso- to Neoarchean in age (Machado et al., 1992; Noce et al., 2005; Teixeira et al., 1998, 2017; Lana et al., 2013; Fig. 1). The Rio das Velhas greenstone belt corresponds to the Rio das Velhas Supergroup, that includes: (i) the Nova Lima Group, a marine succession of mafic-ultramafic metavolcanics, banded iron formations, metasiliciclastics, and felsic metavolcaniclastics whose crystallization ages are between 2792 and 2751 Ma; and (ii) the Maquiné Group, an overlying near-shore, non-marine succession of metasiliciclastic rocks deposited only after ca. 2730 Ma (Baltazar and Silva, 1996; Baltazar and Zucchetti, 2007; Dorr, 1969; Noce et al., 2005; Moreira et al, 2016; Zucchetti et al., 1998). The greenstone rocks were deformed and metamorphosed under greenschist- to lower amphibolite-facies conditions, from the Archean to the Neoproterozoic (Baltazar and Zucchetti, 2000; 2007). The main units of the metamorphic complexes are: (i) usually folded, migmatized, and metamorphosed under amphibolite- to granulite-facies gneisses geochemically akin to TTGs (Engler et al., 2002; Farina et al., 2015; Lana et al., 2013; Machado and Carneiro, 1992; Noce et al., 1997; Teixeira et al., 2017); (ii) crustal-derived high-K metagranitoids (Noce et al., 1997; Carneiro et al., 1998; Farina et al., 2015; Romano et al., 2013); (iii) metaleucogranites with pegmatites (Lana et al., 2013); (iv) minor occurrences of high-K granitic gneisses and mafic-ultramafic layered suites (Goulart et al., 2013; Farina et al., 2015). The complexes and the greenstone are topped by the passive margin to *syn*-orogenic Minas Supergroup, deposited between ca. 2600 and 2100 Ma (Martínez Dopico et al., 2017), cropping out in the Quadrilátero Ferrífero and along the Jeceaba-Bom Sucesso lineament (Neri et al., 2013). Neoproterozoic to Early Ordovician greenschist- to amphibolite-facies metamorphic overprint, and west-verging thrust faults associated with the Brasiliano event (650–480 Ma) are identified in the southeastern

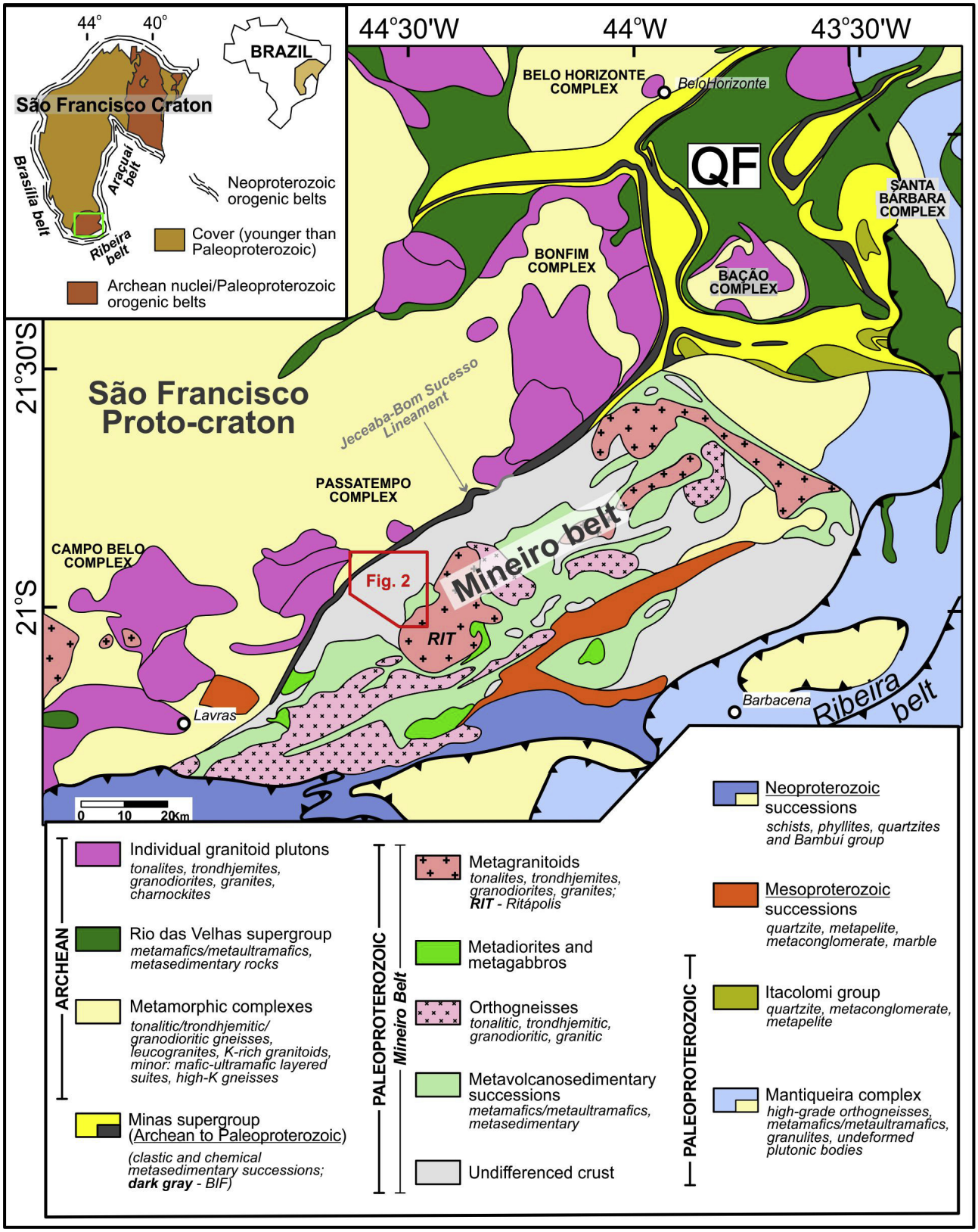

Fig. 1. Geological map of the southernmost São Francisco craton, showing the Archean São Francisco proto-craton and the Paleoproterozoic Mineiro belt. The craton is outlined in its southern border by the Neoproterozoic Brasília and Ribeira belts. QF refers to the Quadrilátero Ferrífero region. The Mantiqueira complex comprises Paleoproterozoic units strongly affected by Neoproterozoic overprint. The Neoproterozoic successions and the Mantiqueira complex may include autochthonous units and allochthonous (Paleoproterozoic and Archean) remnants. Regional geologic contacts were compiled and modified from the Geological map of the Minas Gerais state (CPRM/Codemig, 2014) and published papers (Farina et al., 2015; Romano et al., 2013; Carneiro et al., 2007; Barbosa et al., 2015; Teixeira et al., 2015; Trouw et al., 2013).

margin of the São Francisco Proto-craton (Chemale et al., 1994; Alkmim and Marshak, 1998).

2.2. Mineiro belt

The Mineiro belt is an elongated NE-trending composite orogen developed between ca. 2470 and 2100 Ma, and comprises orthogneisses, metagranitoids, metadiorites, metagabbros, and metasubvolcanic rocks, spatially associated with metavolcano-sedimentary successions (see Alkmim and Teixeira, 2017 for a review; Fig. 1). The rocks from the orogen are associated with a long-lived accretionary regime that evolved to a continental arc to the south of the São Francisco Proto-craton (present coordinates; Ávila et al., 2010, 2014; Teixeira et al., 2015). The units of the Mineiro belt recorded Paleoproterozoic medium amphibolite to greenschist facies metamorphism (Ávila et al., 2010 and references within), contrasting with the complex foliation and metamorphic trajectories that affected the Archean complexes and greenstones.

2.3. Archean to Paleoproterozoic tectono-magmatic evolution (ca. 3300–2100 Ma)

A set of Archean tectono-magmatic events were recognized in the metamorphic complexes, and also as age peaks in the Rio das Velhas and Minas metasedimentary successions (Hartmann et al., 2006; Koglin et al., 2014; Mendes et al., 2014; Moreira et al., 2016; Martínez Dopico et al., 2017). Four events were proposed by Farina et al. (2015); after Lana et al. (2013) for the Quadrilátero Ferrífero, named Santa Bárbara (ca. 3220–3200 Ma), Rio das Velhas I (ca. 2920–2850 Ma), Rio das Velhas II (ca. 2800–2760 Ma), and Mamona (ca. 2760–2680 Ma). Teixeira et al. (2017) suggested a wider sequence of (partially corresponding) events in the southern São Francisco Proto-craton. It includes: (i) a Paleoarchean (> 3.300 Ma) event, indicated by inherited zircon grains and Sm-Nd T_{DM} ages (Teixeira et al., 2017); (ii) Mesoarchean 1 (3220–3200 Ma), Mesoarchean 2 (3050–2920 and 2840 Ma), and Neoarchean 1 (2800–2750 Ma) events, dominated by a juvenile sodic (TTG-akin) magmatism; and (iii) Neoarchean 2 (2720–2700, 2610–2550 Ma), an event of crustal reworking and generation. The TTG and TTG-like rocks were generated by partial melting of basaltic oceanic crust possibly in subduction settings (Campos and Carneiro, 2008; Lana et al., 2013; Noce et al., 1997), with variable amount of interaction with a melt derived by crustal reworking (Farina et al., 2015). The Neoarchean 1 (2800–2750 Ma) was the major event of sodic granitoid magmatism in the Quadrilátero Ferrífero, including the felsic volcanism of the Rio das Velhas greenstone belt, and culminated in a collisional stage ca. 2750 Ma (Farina et al., 2015; Martínez Dopico et al., 2017; Teixeira et al., 2017).

The Neoarchean 2 event (2720–2700 and 2610–2550 Ma) gathered potassic magmatism, which has replaced the sodic magmatism, and crustal thickening and reworking under granulite facies (Farina et al., 2015; Romano et al., 2013; Teixeira et al., 2017). Regional-scale crustal melting in the Quadrilátero Ferrífero generated potassic rocks during the Mamona event ca. 2760–2680 Ma, but a minor stage of high-K magmatism occurred ca. 2610 Ma (Farina et al., 2015; Romano et al., 2013), nearly synchronous with the migmatization of the Passa Tempo Metamorphic Complex (Fig. 1; ca. 2620 Ma for the paleosome, and ca. 2600 Ma for the neosome; Campos et al., 2003). Post-collisonal and/or anorogenic granitoids whose ages are between ca. 2730 and 2650 Ma were also identified in the Campo Belo complex (Moreno et al., 2017). The Archean continent finally cratonized ca. 2600 Ma, and a passive margin sedimentation represented by the Minas Supergroup installed on its borders (Renger et al., 1994; Romano et al., 2013). Continental successions (Caraça Group) graded to platform chemical sedimentation (Itabira Group) between ca. 2600 and 2420 Ma, that were succeeded by the deltaic to shallow water sediments (Piracicaba Group; for a review, see Martínez Dopico et al., 2017).

Paleoproterozoic subduction-related granitoids and metavolcano-sedimentary successions associated with the Mineiro belt supervened the marine successions of the Minas Supergroup. Felsic metaigneous rocks of the Mineiro belt yield three age clusters arcs ascribed to arcs: 2356–2328 Ma, 2227–2204 Ma, and 2192–2121 Ma (Ávila et al., 2010, 2014; Barbosa et al., 2015; Seixas et al., 2012, 2013; Teixeira et al., 2015); the first and the last generated TTGs. Two metamorphic-deformational episodes registered in the Mineiro belt have reached medium amphibolite facies (ca. 2250–2190 Ma), and greenschist to lower amphibolite facies (ca. 2131–2100 Ma; Ávila et al., 2010). On the top of the Minas Supergroup, a foreland succession represented by the Sabará Group had sources from the Mineiro belt, which had collided and uplifted along the São Francisco continental margin after ca. 2120 Ma, converting the latter into an active system (Alkmim and Teixeira, 2017; Machado et al., 1996; Martínez Dopico et al., 2017). The corresponding Paleoproterozoic tectono-metamorphic episodes are evidenced by amphibolite-facies metamorphism, partial melting, and metamorphic titanite and monazite ages of ca. 2100–1950 Ma in the complexes of the Quadrilátero Ferrífero (Aguilar et al., 2017; Machado et al., 1992, 1996; Noce et al., 1998). The extensional collapse of the orogen originated the dome-and-keel framework observed in the Quadrilátero Ferrífero: crustal metamorphic nuclei partially or entirely outlined by supracrustals (Alkmim and Marshak, 1998).

3. Analytical techniques

3.1. Sampling and petrography

We have performed detailed geological mapping of the São Tiago region at the 1:25,000 scale (Fig. 2). In scant outcrops, which have been preserved from the intensive weathering, samples for laboratory studies were selected. Ninety-seven thin sections of different lithotypes were produced, from which textural relationships and mineralogy were obtained by optical mineralogy including modal point-counting.

3.2. Geochemistry

Thirty-three samples of metaigneous rocks, including xenoliths that crop out in the São Tiago area, were analyzed in the Laboratory of Analytical Geochemistry of the University of Campinas (UNICAMP) using a Philips PW 2404 X-ray fluorescence spectrometer for major oxides and trace elements. Seventeen samples were analyzed for REE and other trace elements using a quadrupole ICP-MS, seven samples at Acme and ten samples at UNICAMP. Duplicate analyses showed comparable results between the laboratories.

All samples were reduced to < 200-mesh grain size in an agate disc mill after crushing. The analytical routine for major and trace elements comprised X-ray spectrometry using fusion beads, following the procedures of Vendemiatto and Enzweiler (2001). Trace and REE elements were analyzed by ICP-MS at Acme (Agilent 7500a with a shield torch) and at UNICAMP (Thermo X series 2 quadrupole) after acid digestion.

3.3. Geochronology

Samples were crushed and powdered to approximately 300 μm. Heavy mineral concentrates were obtained by panning and were subsequently purified using bromoform and a Frantz Isodynamic Magnetic Separator. Zircon grains were selected from the least magnetic fraction, loaded into 1-inch diameter epoxy mounts, polished, and cleaned using 10% v/v HNO_3 and deionized water.

Cathodoluminescence imaging on zircon grains and the analytical work were performed at the Institute of Geosciences, UNICAMP. Isotope data were acquired on an ICP-MS Element XR (Thermo Scientific), coupled with an Excite.193 (Photon Machines) laser ablation system equipped with a two-volume HelEx ablation cell. The acquisition protocol followed Navarro et al. (2015) with details in Verma

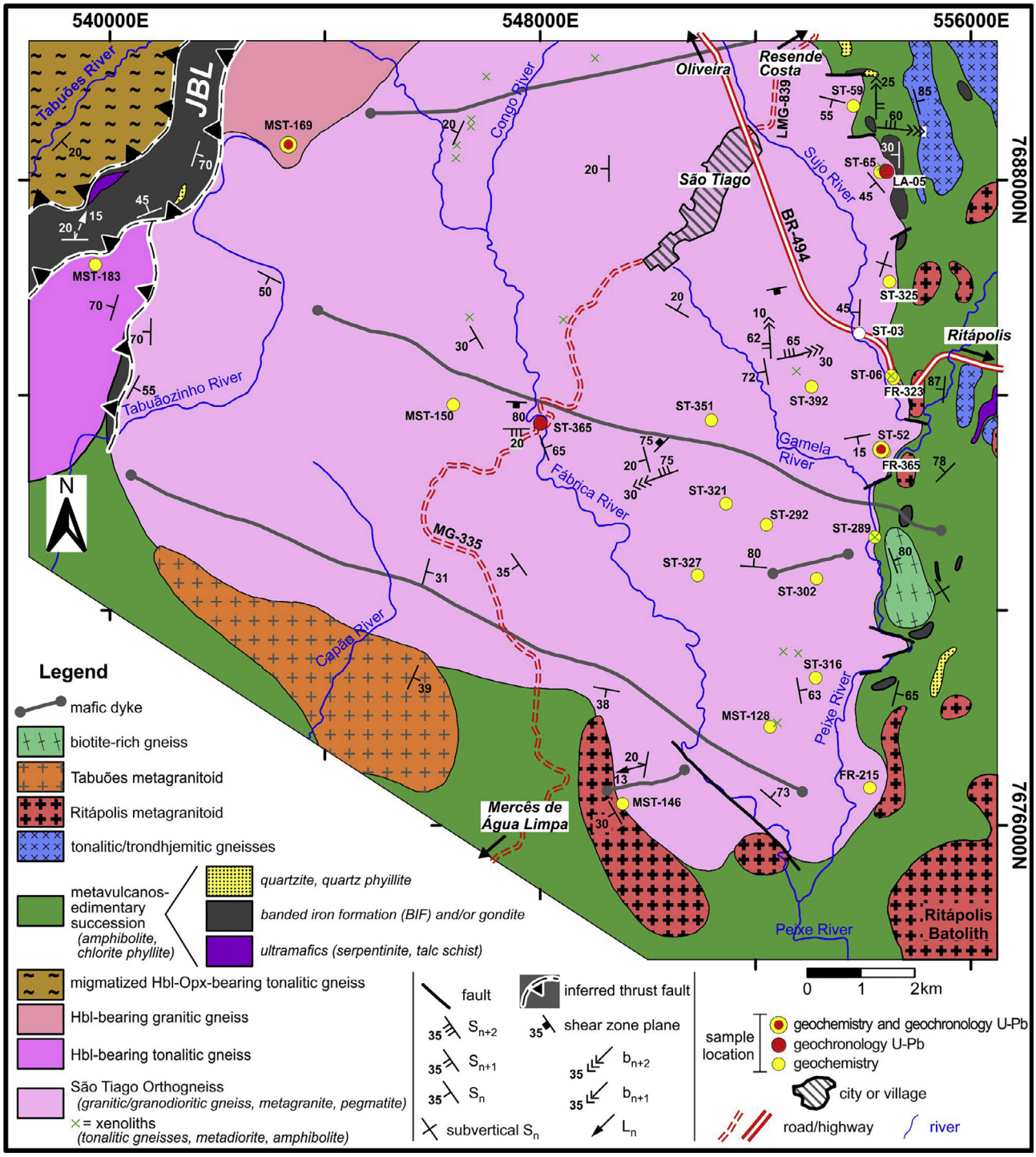

Fig. 2. Geological map of the São Tiago orthogneiss and adjacent rocks. Note the Jeceaba-Bonsucesso lineament (JBL), represented by a metavolcano-sedimentary succession to the northwest of the São Tiago Batholith.

et al. (2016) – laser frequency at 10 Hz, spot size of 40 μm, and laser fluence of 4.74 J cm^{-2}. Data were reduced offline using the Iolite software (version 2.5) following the method of Paton et al. (2010), which involved subtraction of a gas blank followed by a downhole fractionation correction based on the behavior of the 91,500 reference zircon (Wiedenbeck et al., 1995). The obtained 91,500 ages are consistent, within uncertainty, with the ID-TIMS value reported by Wiedenbeck et al. (1995). The $^{207}Pb/^{235}U$ ratios were calculated based on the $^{238}U/^{235}U$ ratio 137.88. The displayed uncertainties are only internal 2 S.E. The Peixe zircon standard (ID-TIMS age of 564 ± 4 Ma; cf. Dickinson and Gehrels, 2003) was used to monitor the quality of the reduction procedures. The $^{206}Pb/^{238}U$ and $^{207}Pb/^{235}U$ ages for Peixe during four sessions of analyses were 566 ± 7 and 566 ± 9, respectively. The analyses of three of the four samples were ^{204}Pb-corrected; all of them were accomplished using Vizual Age version 2014.10 (Petrus and Kamber, 2012) for Iolite, taking into consideration the actual measurement of ^{204}Pb. Samples with a great number of spots with > 1% common Pb had the isotope ratios and ages all corrected for common Pb. On the other hand, samples with a few spots with > 1% common Pb had these spots not considered for age calculation.

4. Results

4.1. Geology of the São Tiago Batholith

The study area comprises a complex tectonic arrangement of Archean and Paleoproterozoic rocks, where the São Tiago Batholith is the main body (ca. 170 km^2) surrounded by a metavolcano-sedimentary succession to the east and south (Fig. 2). At the northwest edge, the São Tiago Batholith is in tectonic contact with rock slivers of supracrustal rocks from the Minas Supergroup that occur along the Jeceaba-Bom Sucesso lineament (Campos and Carneiro, 2008; Neri et al., 2013 and references therein). Two other granitoid bodies have been mapped near the São Tiago Batholith to the northwest and west. The metavolcano-sedimentary succession that encompasses the São Tiago Batholith is crosscut by Paleoproterozoic intrusions related with the Mineiro belt, such as the Ritápolis (2149 ± 10 Ma; Barbosa et al., 2015) and Tabuões metagranitoids, and tonalitic-trondhjemitic gneisses and a biotite-rich gneiss of unknown ages (see Fig. 2). Finally, two sets of NW- and NE-trending mafic dikes crosscut the São Tiago Batholith, the Ritápolis metagranitoid and the supracrustal succession.

4.1.1. Field and petrographic features of the studied units

Four different lithotypes of orthogneissic rocks occur within the São Tiago Batholith, showing complex crosscutting relationships between them (Fig. 3a):

(i) L1 was identified in the center and eastern border of the batholith. It consists of gray to dark gray, fine- to medium-grained, foliated tonalitic orthogneiss (Fig. 3a and b; Fig. 4). The texture is granolepidoblastic. The dominant mineralogy includes quartz, andesine, biotite$_1$ and rare microcline (Fig. 5a). The average color index (M'), between 10 and 40%, reflects the range of the biotite content, which allowed us to distinguish a biotite rich group (Bt-rich) and a biotite poor one (Bt-poor), of distinct geochemistry (see Section 4.2). Apatite, zircon, allanite, opaque minerals and rare rutile and epidote$_1$ are accessory minerals. The secondary mineralogy (i.e., metamorphic or hydrothermal) includes sericite, epidote$_2$, biotite$_2$, chlorite, titanite, and calcite (Fig. 5b). Quartz occurs mainly as recrystallized monomineralic aggregates, and plagioclase crystals are locally recrystallized and kinked (Fig. 5c). Myrmekitic and perthitic/antiperthitic intergrowths are common.

(ii) L2 is the predominant lithotype in the São Tiago Batholith, showing sharp, concordant contact with L1, although the intrusive relations are unclear. It is a whitish, fine- to medium-grained, foliated to banded orthogneiss (Fig. 3a and b) of monzogranitic to granodioritic composition (Fig. 4). The texture is mostly equigranular (locally porphyritic) and granolepidoblastic with M' = 10%. The essential mineralogy consists of andesine, microcline, quartz, and biotite, and the accessory and secondary mineralogies are similar to those observed in L1 (Fig. 5d). Various microcline/andesine ratios reflected in the composition, and permitted a subdivision into two groups of distinct geochemistry (see also Section 4.2): a granodioritic and a granitic one. Diffuse zones of felsic composition are randomly distributed in a few outcrops (Fig. 3c).

(iii) L3 comprises coarse-grained, hololeucocratic pegmatites composed of K-feldspar, plagioclase, quartz and rare muscovite. They occur as centimetric to metric dikes and veins conformably deformed along the main foliation (S_n) of lithotypes 1 and 2 (Fig. 3a, d and e).

(iv) L4 crops out as irregular, centimetric to meter-thick dikes and stocks crosscutting the previous lithotypes (Fig. 3a and d). The rock is a medium-grained, hololeucocratic, isotropic to weakly foliated monzogranite (Fig. 4). It shows isogranular texture with M' = 2%. Microcline, oligoclase, and quartz are the dominant minerals (Fig. 5e). Accessories are biotite$_1$, opaque minerals, apatite, allanite, zircon and rare epidote$_1$. The secondary mineralogy includes sericite, epidote$_2$, biotite$_2$, chlorite, titanite and calcite. Quartz occurs as recrystallized monomineralic aggregates or as single crystals, and plagioclase locally shows reaction borders with microcline, where perthitic intergrowth is developed.

Three structural surfaces are identified in the São Tiago Batholith (Figs. 2 and 3e): (i) the gneissic banding or foliation (S_n); (ii) axial planes of tight to isoclinal folds (S_{n+1}), usually subparallel to S_n; and (iii) axial planes of open folds (S_{n+2}) that affect the S_n and S_{n+1} foliations. There is no unequivocal evidence to support S_n and S_{n+1} as related to different deformation events or part of a single progressive one. S_n contains disrupted or boudined layers and shows mostly N-S strike, although it is quite variable due to later deformational phases. The scarce D_{n+1} axial planes show mostly N-S strike and fold axes plunging at low angles to the north. D_{n+2} axial planes show E-W strike with fold axes plunging at low angles to the east or west.

Deformed xenoliths of hornblende-bearing tonalitic gneiss (Fig. 3f) and scarce pyroxene-bearing diorite and amphibolite occur in the L2, L3, and L4 lithotypes, which suggests that the São Tiago Batholith intruded older crust (discussed in later sections). The tonalitic xenoliths are dark gray, fine- to medium-grained, and foliated, with average M' of 40%, and are composed of biotite$_1$, andesine, quartz, hornblende and rare microcline (Fig. 5f). Apatite, zircon and opaque minerals are accessory minerals, while sericite, epidote$_2$, biotite$_2$, chlorite, and titanite are the secondary minerals.

A hornblende-bearing (Hbl-bearing) granitic gneiss is mapped at the northwest edge of the São Tiago Batholith. Because the geologic relationships with the main body are not clear, we selected a sample for U-Pb dating. The gneiss comprises light gray, medium-grained, foliated to banded orthogneisses of monzogranitic composition (Fig. 4). The texture is mostly equigranular and granolepidoblastic, and M' = 8%. The dominant mineralogy includes microcline, oligoclase, and quartz; mafic phases are biotite$_1$ and minor hornblende. Apatite, zircon, opaque minerals, epidote$_1$, and clinozoisite are the accessory minerals, and sericite, epidote$_2$, chlorite, and biotite$_2$ are the secondary ones.

In the NW, the São Tiago Batholith is in tectonic contact, possibly by a thrust fault, with BIF slivers that likely belong to the Minas Supergroup and a hornblende-bearing (Hbl-bearing) tonalitic gneiss (Fig. 2). The geologic relations suggest this gneiss does not belong to the São Tiago Batholith. The lithotype includes gray, medium-grained foliated orthogneisses of tonalitic composition. It is composed of quartz, andesine and rare microcline; hornblende and biotite$_1$ (in equal proportions) are the mafic phases. The accessory minerals comprise epidote$_1$, apatite, rutile, opaque and zircon; the secondary minerals are sericite, muscovite, epidote$_2$ and biotite$_2$. The texture is granolepidoblastic (Fig. 5f), and M' = 20%.

4.2. Whole-rock geochemistry

Whole-rock geochemical analyses were performed on samples of the São Tiago Batholith as follows: L1 (n = 9), L2 (n = 14) and L4 (n = 6) lithotypes. In addition, the Hbl-bearing granitic gneiss (n = 1), Hbl-bearing tonalitic gneiss (n = 1), and the tonalitic xenoliths (n = 2) were also studied. The results for major, trace and REE elements are shown in Table 1.

Besides distinct color indices, different values of SiO_2, Na_2O, and K_2O observed in the L1 Bt-rich tonalitic gneiss and the L1 Bt-poor tonalitic gneiss (Table 1) were associated with modal biotite content (M' = 10–40%). Similarly, distinct Al_2O_3, Na_2O and K_2O contents in Lithotype 2 reflect various microcline/andesine ratios, and also supported its division into L2 granodioritic gneiss and L2 granitic gneiss.

Using the normative feldspar classification diagram (Fig. 6a), the L1 Bt-rich tonalitic gneiss plots mostly in the granodiorite field, associated with its higher biotite content, while the L1 Bt-poor tonalitic gneiss is classified as a trondhjemite, as a result of its low proportion of that

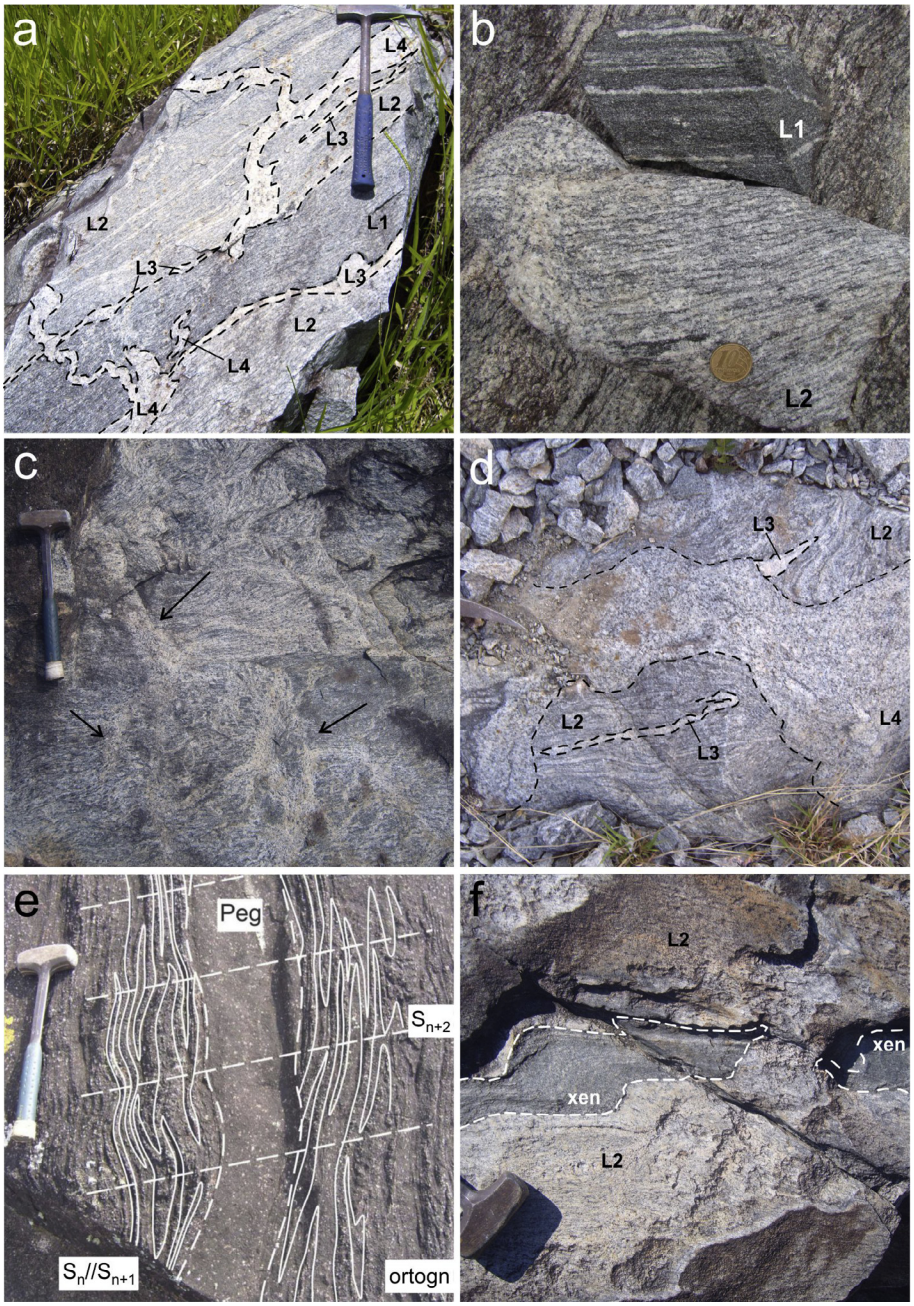

Fig. 3. Field aspects of the São Tiago Batholith and related units. (a) Crosscutting relations between the described lithotypes: L4 is intrusive in L3, which is sub-concordant with both the L1 and L2 foliation. (b) Hand sample aspects of the L1 (grayish fine-grained foliated) and the L2 (whitish medium-grained banded) orthogneisses. (c) Medium-grained, slightly foliated L4 metagranite that crosscuts L3, which in turn is folded concordantly with the main L2 foliation. (d) Migmatitic aspect of L2, represented by diffuse zones of leucocratic composition (arrows). (e) Deformational structures of the São Tiago orthogneiss: gneissic banding or foliation (S_n), tight to isoclinal folds with axial plane (S_{n+1}) subparallel to S_n, and open folds (S_{n+2}) that affect S_n and S_{n+1}. (f) Folded and boudined xenolith of a tonalitic gneiss in the L2 granitic gneiss.

mineral. The L2 granodioritic gneiss plots in both the granite and the trondhjemite fields (linked with variable microcline/plagioclase ratio). The L2 granitic gneiss, the L4 metagranite, and the Hbl-bearing granitic gneiss plot only in the granite field due to their higher microcline contents. The Hbl-bearing tonalitic gneiss and one sample of the tonalitic xenolith are classified as tonalite, whereas the other xenolith (ST-65-2B) is classified as granodiorite.

The major element contents of the analyzed rocks are highly variable (Table 1). The L1 Bt-rich tonalitic, the Hbl-bearing tonalitic gneiss, and the xenoliths present the lowest values of silica; the L1 Bt-poor tonalitic, the Hbl-bearing granitic, and the L2 granodioritic gneiss are more acid; and the L2 granitic gneiss and L4 metagranite exhibit the highest values of SiO_2. The L1, L2, and L4 lithotypes display a fairly wide distribution of Al_2O_3 contents, reflecting in a disperse pattern in the A/CNK vs A/NK diagram, although most samples are slightly peraluminous (Figs. 6b and 7a). The Hbl-bearing tonalitic gneiss, the xenoliths, and two samples of the L1 Bt-rich tonalitic gneiss are metaluminous and iron- and magnesium-richer than the other lithotypes (Fig. 7b). FeO_t + MgO and CaO values are moderate to high for L1, and low for L2 and L4; most of the L1 and L2 lithotypes show a negative correlation between silica and those oxides (Fig. 7b and c). The L1 Bt-poor tonalitic gneiss and most of the L2 granodioritic gneisses display high Na_2O values and plot in the medium-K field in the K_2O vs. SiO_2 diagram (Fig. 7d and e). The L1 Bt-rich tonalitic gneiss, the L2 granitic gneiss, and the L4 metagranite have low to moderate Na_2O and moderate to high K_2O, plotting in the fields of the high-K calc-alkaline to shoshonitic series due to the higher biotite content in the first and higher microcline in the other two types (Fig. 7d and e). Only the L1 Bt-rich tonalitic gneiss shows a negative correlation between K_2O and SiO_2 (Fig. 7e). The L1 Bt-poor gneiss, the Hbl-bearing tonalitic gneiss, and one of the xenoliths present low values of K_2O/Na_2O; the L1 tonalitic gneiss, the L2 granodioritic gneiss and the other xenolith display moderate values of such ratios; the remnant samples exhibit high values (Fig. 7f).

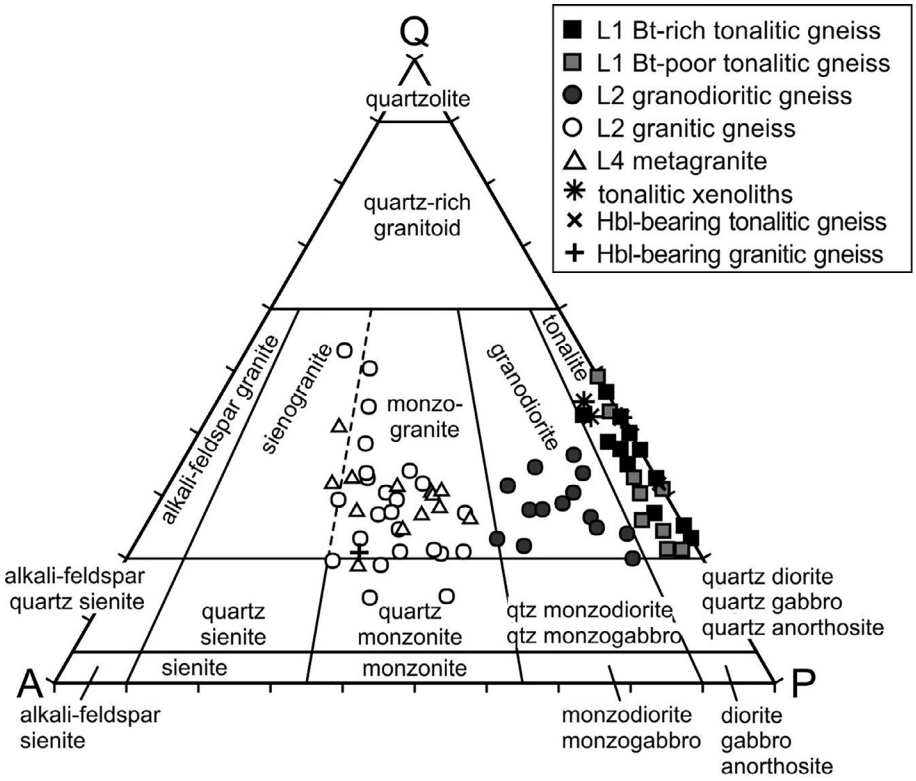

Fig. 4. QAP diagram of Streckeisen (1976) showing the composition of São Tiago gneisses and metagranites, and other studied gneisses. Mineral abundance obtained by point-counting.

Most lithotypes present overall low to moderate Ba, moderate to high Rb, and intermediate Sr contents, producing negative Ba anomalies and variable Rb and Sr anomalies, and fractioned REE patterns with negative Eu anomalies (Table 1; Figs. 8 and 9). Exceptions are the Hbl-bearing tonalitic gneiss and a single L1 Bt-poor tonalitic gneiss sample (ST-327A), which lack Eu anomaly, and are Sr- and Ba-rich but Rb-poor, reflecting in positive Ba anomalies (Fig. 8a and b). The L1 Bt-rich tonalitic gneiss and the L4 metagranite show flatter REE patterns, although the former presents overall high REE, and the latter, low REE. Considering the HFSE contents, all lithotypes also display negative Nb and Ti anomalies, which are more marked for the L2 granitic gneiss and the L4 metagranite, and low to moderate values of Th, but higher for these two cited types and for the Hbl-bearing tonalitic gneiss (Fig. 8b–d). Similar spider diagram patterns are found in both the L2 granodioritic and the Hbl-bearing tonalitic gneisses, but these lithotypes show higher negative anomalies for Ta in the former and for Nb in the latter (Fig. 8b). Trace element amounts of the Hbl-bearing granitic gneiss are comparable to theirs of L2 granitic gneiss, but the former presents slightly higher Y, Zr and Nb values, and slightly lower Th values (Table 1). Remarkable trace element differences between the L1 Bt-rich tonalitic and the L1 Bt-poor tonalitic gneisses are higher Rb, Y, and HREE, lower Sr, absence of negative P anomaly, and presence of positive U anomaly in the former (Figs. 8a and 9a).

4.3. Geochronology

In situ zircon LA-ICP-MS dating was performed on metaigneous rocks L1 Bt-rich tonalitic gneiss, L2 granitic gneiss, and L3 pegmatite, as well as on the Hbl-bearing granitic gneiss that occurs between the São Tiago Batholith and the Jeceaba-Bom Sucesso lineament. The U-Pb analyses are presented in Table S1 of the Supplementary Data. The CL images for selected zircon grains from the analyzed samples and the Concordia diagrams are presented in Figs. 10 and 11, respectively.

In general, zircon crystals are typically prismatic (up to 5:1 in length:width ratios) and between 60 and 500 μm in length. Most of the crystals are metamictic with mineral inclusions and show dark overgrowths and partly resorbed nuclei. The acquired isotopic data show large scatter due to variable and complex Pb loss, likely associated with the polycyclic history of the investigated samples. It may have been linked with Neoarchean and Paleoproterozoic magmatism/metamorphism, and younger overprints identified in U-Pb plot regressions to imprecise Neoproterozoic/Cambrian ages.

Sample ST-365 is an L1 Bt-rich tonalitic gneiss sample collected at the core of the São Tiago Batholith (Fig. 2; 548005/7683486 UTM). The zircon grains from this sample are light pink to pale brown, rounded or prismatic (3:1) with a maximum length of 250 μm. Inclusions of Fe-Ti oxides are common. Zircon grains show low luminescence and oscillatory zoning interpreted as indicating igneous origin (Fig. 10a). Due to scattered data, we selected seven aligned ellipses with the youngest ages and > 70% concordant, defining an upper intercept age at 2816 ± 30 Ma with MSDW of 3.2 (Fig. 11a). It is considered the crystallization age of the rock. Several zircon grains yield Neoarchean $^{207}Pb/^{206}Pb$ ages, whereas a few older, mostly discordant $^{207}Pb/^{206}Pb$ ages, sometimes as igneous cores (e.g., ST-365–4; Fig. 10a) are interpreted as inherited.

Sample ST-52 is an L2 K-rich granitic gneiss collected at the eastern exposure of the São Tiago body (Fig. 2; 554335/7682954 UTM). The zircon grains are milky white and purple to pale brown and prismatic (up to 4:1) or stubby, 400 μm in length at most. In CL images, most of the crystals show concentric or irregular oscillatory zoning (Fig. 10b), interpreted as indicating igneous origin. Fifteen analyses < 5% discordant produce an upper intercept age of 2671 ± 7 Ma (MSWD = 2.9), equivalent within errors to the weighted mean age of 2664 ± 4 Ma (MSWD = 1.3) for a subset of ten analyses, excluding five outliers. Finally, we identify no inherited zircon in CL images, so the former age is interpreted as the crystallization age of this granitic gneiss.

Sample LA-05 is an L3 pegmatite that crosscuts L2 K-rich granitic

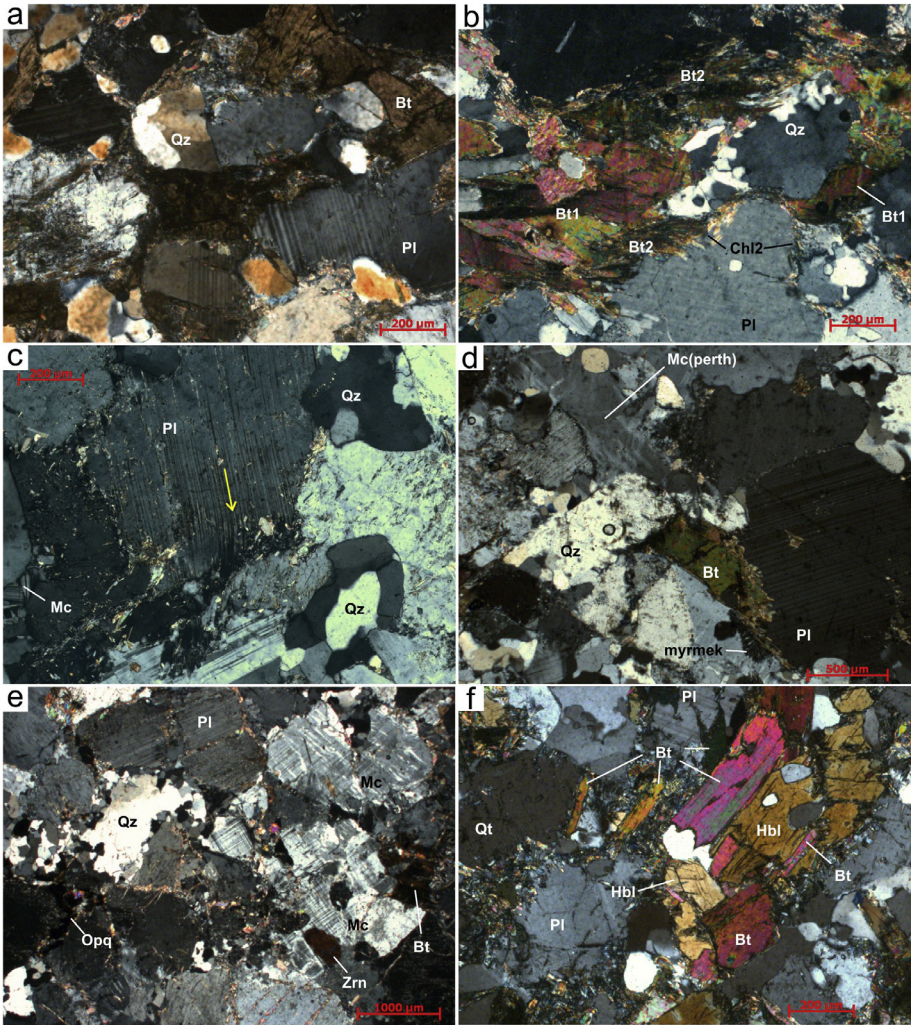

Fig. 5. Petrographic features of gneisses and metagranites from the São Tiago region. All images are with crossed-polarizes. (a) Essential mineralogy of L2. (b) Alteration minerals common in both L1 and L2; note petrographical differences between biotite$_1$ and biotite$_2$. (c) Kinked lamellae of plagioclase, evidencing solid-state deformation. (d) Essential mineralogy of L1; note myrmekitic and perthitic intergrowths and recrystallized quartz. (e) L4 mineralogy; note the large crystal of microcline and the diversity of mafic minerals (biotite and opaque minerals). (f) Cluster of biotite and hornblende of the Hbl-bearing tonalitic gneiss. Mineral abbreviations are after Whitney and Evans (2010). Additional abbreviations: *myrmek* = myrmekite; *perth* = perthite.

gneiss at the northeastern exposure area of the São Tiago body (Fig. 2; 554430/7688167 UTM). The zircon grains are white or light pink to pinkish-brown, prismatic (up to 2:1) and stubby, and up to 350 µm in length. In the CL images, most of the crystals show concentric oscillatory zoning, interpreted as indicating igneous origin (Fig. 10c). A selection of six concordant and subconcordant grains with oscillatory or sector zoning – up to 10% discordant – define an upper intercept age of 2657 ± 23 Ma (MSWD = 5.0). It is considered the crystallization age of the rock (Fig. 11c). A significant older zircon population is also apparent in the U-Pb plot, although related to scattered discordant data (see Supplementary Table S1).

Sample MST-169-A was collected to the northwest of the São Tiago body (Fig. 2; 543311/7688622 UTM). The rock is classified as hornblende-bearing monzogranitic gneiss, locally migmatized. The zircon crystals are white to light gray and pale to dark brown, prismatic (up to 4:1) or stubby, and up to 650 µm in length. Many grains are metamictic/turbid with inclusions of apatite and Fe-oxides. The CL images (Fig. 10d) show patchy oscillatory or sector zoning in most of the analyzed crystals; a subset of crystals is homogeneously dark with no internal zoning. Partly resorbed cores are also present. The data show significant scatter in the U-Pb diagram. We selected the five least discordant (up to 20%) grains with the same internal zoning characteristics, likely igneous in origin to yield an upper intercept age of 2614 ± 13 Ma (MSWD = 1.1; Fig. 11d), recognized as the crystallization age of the rock.

5. Discussion

This section integrates the field, mineralogical, geochemical and geochronological data of this work with information from the literature to discuss nomenclature, petrogenesis and regional geotectonic implications. Table 2 presents a summary of the geochemical characteristics of metagranitoids from the São Tiago region along with compiled data from similar rocks of the Quadrilátero Ferrífero for the petrogenetic inferences.

5.1. Classification of the lithotypes

Laurent et al. (2014) suggested a useful classification diagram that discriminates the four types that they proposed to constitute most Late Archean granitoids: TTGs, biotite and two-mica granites, sanukitoids, and hybrid granitoids (Fig. 12a). The classification indicated by our rock plots in this diagram is not definitive, but instead illustrates the most possible major group type to which our rocks belong, refined using other geochemical parameters and diagrams.

In that diagram, the L1 Bt-poor tonalitic gneiss plots in the TTG field (Fig. 12a) and as trondhjemite in the O'Connors' diagram (Fig. 6). Indeed, this gneiss is chemically akin with trondhjemites, but slight variations regarding its biotite contents (> 10%) preclude a precise nomenclature for this rock. The contents of Sr and Sr/Y are lower and the ferromagnesian oxides are higher than TTG s.s. (cf. Moyen, 2011; Moyen and Martin, 2012). The chemical characteristics of most L1 Bt-poor tonalitic gneisses correspond to low- and medium-pressure

Table 1
Major, trace and rare earth element data for selected orthogneisses and metagranites from the São Tiago region.

Rock type	L1 Bt-rich tonalitic gneiss					L1 Bt-poor tonalitic gneiss				L2 granodioritic gneiss							L2 granitic gneiss
Sample	FR-215-2A	ST-59	ST-59-2B	ST-65-2C	ST-65D	FR-323	MST-128H	ST-65-2A	ST-327A	FR-325	FR-359	MST-146A	MST-150	ST-03	ST-06C	ST-289A	FR-365B1
Major elements (wt%)																	
SiO_2	67.31	65.55	65.09	62.59	58.99	70.07	68.47	66.73	66.21	69.05	71.06	72.97	72.75	70.28	72.52	71.92	71.92
TiO_2	0.88	0.96	0.99	0.73	0.88	0.43	0.40	0.58	0.44	0.57	0.62	0.13	0.20	0.49	0.25	0.25	0.41
Al_2O_3	14.13	14.97	14.94	15.11	15.47	15.04	16.18	15.31	16.46	14.95	14.09	15.49	14.73	14.63	15.18	14.94	13.45
FeO_t	5.14	5.24	5.32	6.56	8.15	2.61	2.40	4.71	4.21	3.49	3.03	0.90	1.45	3.29	1.64	1.61	2.53
MnO	0.11	0.09	0.09	0.13	0.17	0.06	0.05	0.08	1.05	0.06	0.04	0.02	0.03	0.06	0.03	0.03	0.05
MgO	1.62	1.76	1.84	2.63	3.46	1.21	1.22	1.19	0.06	1.26	1.13	0.28	0.51	0.99	0.57	0.60	0.71
CaO	2.14	2.92	2.91	4.14	4.44	2.66	2.63	3.06	3.22	2.16	2.09	1.67	2.37	1.86	1.92	1.80	1.57
Na_2O	4.11	3.81	3.45	3.41	2.93	4.88	5.11	4.70	5.36	4.72	3.87	5.94	4.67	4.27	4.69	4.75	3.41
K_2O	2.37	2.76	2.97	2.58	3.30	1.56	1.74	1.76	1.31	2.55	2.90	1.91	1.84	3.34	3.11	2.77	4.77
P_2O_5	0.24	0.30	0.30	0.28	0.34	0.12	0.18	0.25	0.14	0.17	0.21	0.06	0.07	0.11	0.06	0.09	0.11
LOI	1.15	0.96	1.22	0.88	0.94	0.58	0.97	0.58	1.20	0.62	0.61	0.39	0.77	0.33	0.42	0.70	0.34
Trace elements (ppm)																	
V	62.0	67.5	82.0	66.0	85.3	42.1	33.0	30.0	48.0	55.1	43.5	7.0	12.0	50.0	28.0	15.9	32.0
Cr	50.0	23.7	20.0	55.0	46.7	3.1	23.4	13.0	< 5	7.5	18.6	6.2	4.4	< 5	< 5	15.2	n.d.
Ni	18.2	11.1	11.7	37.0	45.4	10.9	15.3	6.9	3.6	7.6	10.4	< 2	2.1	40.0	41.0	6.0	4.1
Rb	243.0	221.3	241.0	174.0	242.2	43.5	142.0	129.0	43.7	116.0	45.4	90.0	85.0	213.0	150.0	111.5	196.0
Sr	161.0	233.3	241.0	253.0	230.6	213.7	423.0	253.0	777.9	182.0	84.2	364.0	279.0	186.0	451.0	443.8	113.0
Y	75.0	46.7	49.0	25.8	32.8	13.7	18.3	23.9	26.5	10.3	36.5	8.3	10.6	31.0	23.0	8.9	43.0
Zr	530.0	465.6	358.0	130.0	148.6	161.2	153.0	149.0	208.6	342.4	367.3	100.0	118.0	330.0	172.0	115.5	175.0
Nb	26.5	15.1	24.5	13.6	13.7	9.2	15.4	15.7	7.3	15.7	8.0	11.9	12.9	41.0	26.0	6.0	20.8
Ba	254.0	382.9	387.0	249.0	233.9	166.2	462.0	232.0	1024.0	403.4	768.9	179.0	360.0	798.0	822.0	564.5	624.0
Hf	n.d.	12.0	n.d.	n.d.	3.6	3.4	n.d.	n.d.	5.4	8.5	9.2	n.d.	n.d.	n.d.	n.d.	3.3	n.d.
Ta	n.d.	0.8	n.d.	n.d.	1.5	0.6	n.d.	n.d.	1.2	0.4	0.1	n.d.	n.d.	n.d.	n.d.	0.9	n.d.
Pb	21.5	13.6	14.2	15.3	14.9	11.1	14.2	14.8	3.3	12.8	11.3	23.5	23.5	n.d.	n.d.	16.9	29.5
Th	12.9	14.1	12.8	3.3	4.2	7.3	6.1	6.9	15.4	19.3	12.7	4.0	6.0	n.d.	n.d.	4.8	31.0
U	n.d.	4.5	n.d.	n.d.	1.9	0.8	n.d.	n.d.	1.4	1.9	2.6	n.d.	n.d.	n.d.	n.d.	0.4	n.d.
La	59.0	72.6	61.0	17.0	19.4	39.6	17.0	14.0	52.5	96.4	47.2	< 13	14.0	n.d.	n.d.	30.2	64.0
Ce	122.0	138.9	131.0	46.0	41.0	54.7	32.0	51.0	79.5	161.1	87.2	< 13	21.0	n.d.	n.d.	45.7	159.0
Pr	n.d.	15.2	n.d.	n.d.	5.1	7.4	n.d.	n.d.	8.9	17.4	10.5	n.d.	n.d.	n.d.	n.d.	5.6	n.d.
Nd	64.0	57.6	68.0	22.0	19.7	25.1	< 11	25.0	29.1	51.8	36.9	< 11	< 11	n.d.	n.d.	19.2	62.0
Sm	n.d.	10.4	n.d.	n.d.	4.9	5.4	n.d.	n.d.	5.7	6.9	8.0	n.d.	n.d.	n.d.	n.d.	2.7	n.d.
Eu	n.d.	1.4	n.d.	n.d.	1.2	0.8	n.d.	n.d.	1.6	0.7	1.2	n.d.	n.d.	n.d.	n.d.	0.8	n.d.
Gd	n.d.	9.8	n.d.	n.d.	4.7	4.0	n.d.	n.d.	4.7	5.2	7.0	n.d.	n.d.	n.d.	n.d.	2.3	n.d.
Tb	n.d.	1.6	n.d.	n.d.	0.9	0.5	n.d.	n.d.	0.8	0.5	1.1	n.d.	n.d.	n.d.	n.d.	0.3	n.d.
Dy	n.d.	8.7	n.d.	n.d.	5.5	2.8	n.d.	n.d.	4.9	2.1	6.8	n.d.	n.d.	n.d.	n.d.	1.6	n.d.
Ho	n.d.	1.6	n.d.	n.d.	1.1	0.5	n.d.	n.d.	0.9	0.4	1.3	n.d.	n.d.	n.d.	n.d.	0.3	n.d.
Er	n.d.	4.6	n.d.	n.d.	3.2	1.3	n.d.	n.d.	3.1	1.0	3.6	n.d.	n.d.	n.d.	n.d.	0.8	n.d.
Tm	n.d.	0.6	n.d.	n.d.	0.5	0.2	n.d.	n.d.	0.5	0.1	0.5	n.d.	n.d.	n.d.	n.d.	0.1	n.d.
Yb	n.d.	3.9	n.d.	n.d.	3.2	1.0	n.d.	n.d.	2.7	0.7	3.1	n.d.	n.d.	n.d.	n.d.	0.7	n.d.
Lu	n.d.	0.5	n.d.	n.d.	0.5	0.1	n.d.	n.d.	0.4	0.1	0.5	n.d.	n.d.	n.d.	n.d.	0.1	n.d.

(*continued on next page*)

Table 1 (*continued*)

Rock type	L2 granitic gneiss		Rock type	L2 granitic gneiss				L4 metagranite						Hbl-bearing granitic gneiss	Hbl-bearing tonalitic gneiss	tonalitic xenoliths	
Sample	ST-52B	ST-65B	Sample	ST-292B	ST-321	ST-351A	ST-351B	FR-365A	FR-365B2	ST-06A	ST-65Y	ST-272	ST-316	MST-169B	MST-183	ST-06X	ST-65-2B
Major elements (wt%)			*Major elements (wt%)*														
SiO_2	73.18	70.95	SiO_2	73.67	71.06	77.35	72.94	73.35	75.40	73.04	70.46	73.62	73.10	69.11	62.44	61.49	59.52
TiO_2	0.29	0.39	TiO_2	0.19	0.26	0.14	0.14	0.23	0.13	0.07	0.12	0.14	0.25	0.71	0.51	0.70	0.85
Al_2O_3	13.60	14.22	Al_2O_3	13.72	14.98	12.19	14.71	13.61	12.32	15.33	15.71	14.41	14.11	14.05	15.47	16.06	15.08
FeO_t	1.77	2.65	FeO_t	1.42	1.55	0.79	0.76	1.43	0.95	0.60	0.78	0.92	1.48	3.79	4.91	5.73	7.79
MnO	0.04	0.04	MnO	0.02	0.76	0.26	0.01	0.03	0.02	0.01	0.24	0.37	0.02	0.06	0.09	0.11	0.17
MgO	0.52	0.67	MgO	0.32	0.02	0.01	0.25	0.35	0.21	0.15	0.01	0.03	0.48	0.88	3.08	3.11	3.41
CaO	1.39	1.63	CaO	1.04	1.17	0.89	1.10	1.17	1.04	1.53	1.39	1.28	0.98	2.12	5.03	4.80	4.90
Na_2O	3.26	3.69	Na_2O	3.46	4.02	2.91	3.63	3.26	2.65	4.55	3.69	4.58	2.92	3.47	4.39	4.14	3.02
K_2O	5.25	4.59	K_2O	5.28	5.04	4.90	5.82	5.96	6.36	4.33	6.35	3.49	5.12	4.26	1.80	1.92	2.84
P_2O_5	0.08	0.11	P_2O_5	0.07	0.07	0.02	0.03	0.06	0.05	0.01	0.03	0.04	0.07	0.22	0.24	0.21	0.33
LOI	0.27	0.46	LOI	0.62	0.60	0.20	0.48	0.51	0.53	0.67	0.90	0.80	0.99	0.66	1.14	1.00	0.88
Trace elements (ppm)			*Trace elements (ppm)*														
V	22.2	32.0	V	n.d.	19.0	10.0	6.0	n.d.	18.1	10.0	19.0	13.0	17.0	43.0	87.5	75.0	88.0
Cr	2.1	n.d.	Cr	n.d.	n.d.	n.d.	n.d.	n.d.	1.6	< 5	< 5	< 5	n.d.	16.9	41.2	52.0	72.0
Ni	2.5	4.8	Ni	n.d.	5.2	2.4	2.6	n.d.	0.7	42.0	1.9	2.0	4.4	8.0	42.0	44.0	48.0
Rb	165.1	190.0	Rb	n.d.	191.0	176.0	196.0	n.d.	167.4	170.0	217.8	139.3	200.0	210.0	78.1	113.0	184.0
Sr	95.0	150.0	Sr	n.d.	198.7	124.0	147.0	n.d.	70.0	466.0	171.1	394.1	112.0	153.0	728.2	301.0	228.0
Y	28.6	20.6	Y	n.d.	43.2	14.7	10.8	n.d.	31.6	24.0	9.9	20.2	53.0	73.0	20.1	24.0	28.1
Zr	184.5	265.0	Zr	n.d.	195.3	141.9	146.0	n.d.	99.4	113.0	21.7	82.3	203.0	347.0	172.1	145.0	134.0
Nb	10.3	18.4	Nb	n.d.	15.6	9.4	8.5	n.d.	3.7	24.0	8.7	18.7	16.6	24.1	8.1	22.0	12.9
Ba	670.5	673.0	Ba	n.d.	841.0	464.0	550.0	n.d.	773.8	1094.0	838.0	605.0	682.0	848.0	1421.7	673.0	180.0
Hf	5.0	n.d.	Hf	n.d.	6.0	5.4	n.d.	n.d.	2.7	n.d.	0.6	3.1	n.d.	n.d.	4.0	n.d.	n.d.
Ta	0.3	n.d.	Ta	n.d.	1.8	1.4	n.d.	n.d.	0.2	n.d.	1.9	2.9	n.d.	n.d.	1.1	n.d.	n.d.
Pb	27.1	36.0	Pb	n.d.	19.4	18.7	42.0	n.d.	23.0	n.d.	20.8	12.2	28.5	32.0	26.4	n.d.	14.9
Th	43.1	38.0	Th	n.d.	24.8	47.2	26.0	n.d.	10.1	n.d.	31.8	8.0	44.0	20.0	26.2	n.d.	3.0
U	5.6	n.d.	U	n.d.	3.8	3.8	n.d.	n.d.	2.3	n.d.	10.9	2.5	n.d.	n.d.	4.3	n.d.	n.d.
La	53.0	76.0	La	n.d.	104.5	55.5	33.0	n.d.	18.4	n.d.	27.6	13.0	134.0	67.0	77.2	n.d.	17.0
Ce	98.5	158.0	Ce	n.d.	195.5	114.0	60.0	n.d.	28.5	n.d.	55.0	23.4	174.0	165.0	114.1	n.d.	61.0
Pr	10.9	n.d.	Pr	n.d.	22.5	12.8	n.d.	n.d.	4.1	n.d.	5.6	2.7	n.d.	n.d.	11.6	n.d.	n.d.
Nd	34.9	56.0	Nd	n.d.	75.4	44.4	21.0	n.d.	14.6	n.d.	18.8	10.7	120.0	66.0	36.1	n.d.	30.0
Sm	6.4	n.d.	Sm	n.d.	12.4	8.5	n.d.	n.d.	3.8	n.d.	3.5	2.3	n.d.	n.d.	5.8	n.d.	n.d.
Eu	0.7	n.d.	Eu	n.d.	0.9	0.6	n.d.	n.d.	0.6	n.d.	0.8	0.4	n.d.	n.d.	1.6	n.d.	n.d.
Gd	5.5	n.d.	Gd	n.d.	9.0	6.6	n.d.	n.d.	3.8	n.d.	2.4	2.4	n.d.	n.d.	4.9	n.d.	n.d.
Tb	0.8	n.d.	Tb	n.d.	1.4	0.9	n.d.	n.d.	0.8	n.d.	0.4	0.5	n.d.	n.d.	0.6	n.d.	n.d.
Dy	5.1	n.d.	Dy	n.d.	7.5	3.7	n.d.	n.d.	5.5	n.d.	1.9	3.0	n.d.	n.d.	3.0	n.d.	n.d.
Ho	1.0	n.d.	Ho	n.d.	1.4	0.6	n.d.	n.d.	1.2	n.d.	0.4	0.6	n.d.	n.d.	0.6	n.d.	n.d.
Er	2.8	n.d.	Er	n.d.	3.9	1.3	n.d.	n.d.	3.3	n.d.	0.9	2.1	n.d.	n.d.	1.6	n.d.	n.d.
Tm	0.4	n.d.	Tm	n.d.	0.6	0.1	n.d.	n.d.	0.5	n.d.	0.1	0.3	n.d.	n.d.	0.2	n.d.	n.d.
Yb	2.4	n.d.	Yb	n.d.	3.4	0.6	n.d.	n.d.	3.0	n.d.	0.7	2.6	n.d.	n.d.	1.3	n.d.	n.d.
Lu	0.3	n.d.	Lu	n.d.	0.5	0.1	n.d.	n.d.	0.4	n.d.	0.1	0.4	n.d.	n.d.	0.2	n.d.	n.d.

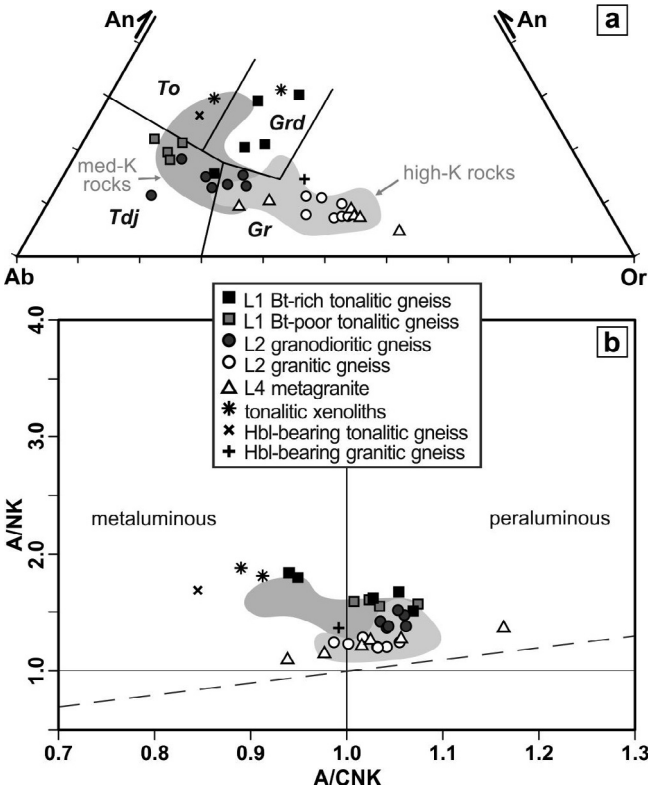

Fig. 6. (a) Normative feldspar classification diagram for granitoids (An-Ab-Or; O'Connor, 1965) with the fields of Barker (1979). (b) A/CNK vs A/NK diagram of Shand (1943). The gray fields refer to medium-K (banded gneiss and plagioclase-rich granitoids) and high-K (K-feldspar-rich granite and K-felspar-bearing gneisses) rocks from the Quadrilátero Ferrífero region, to the NE of the study area. Data from Farina et al. (2015).

Archean TTG that composes part of the Archean gray gneisses of Moyen (2011); Fig. 12(b).

The L1 tonalitic gneiss is geochemically similar to low-silica, high-Ti sanukitoids of Martin et al. (2009); Fig. 12(c), but unlike the broader definition of sanukitoids (Heilimo et al., 2010), the unit presents low Ba, Sr and Sr/Y, flat REE patterns and strong negative [Eu/Eu]*. The new data plot in the field of "hybrid" granitoids (Fig. 12a).

The L2 Na-rich granodioritic gneiss varies from TTGs to hybrid granitoids (Fig. 12a) as a result of the variable potassium content (i.e., modal biotite and K-feldspar). That range of composition also permits that some samples are labeled as medium-pressure TTGs, while others are potassic, according to the Moyen's classification (2011; Fig. 12b). The hornblende-bearing monzogranitic gneiss is also chemically classified as a "hybrid granitoid" (Fig. 12a), while the hornblende-bearing tonalitic gneiss is a sanukitoid, satisfying all the criteria established by Heilimo et al. (2010), and plots specifically into the low-Ti group of Martin et al. (2009); Fig. 12(c). However, due to a shortage of analyzed samples from the latter group, we cannot ensure that the entire body belongs to the sanukitoid series.

On the other hand, the L2 K-rich granitic gneiss and the L4 metagranite plot within the "biotite and two-mica" granite field (Fig. 12a). The geochemical composition of these rocks correlates well with the "potassic" component of Archean gray gneisses described in "late potassic batholiths" worldwide (Feng and Kerrich, 1992; Moyen et al., 2003; Windley, 1995; cf. Fig. 12b and c), including the southern São Francisco Craton (Carneiro et al., 1998; Noce et al., 1997; Romano et al., 2013).

5.2. Regional correlations

5.2.1. Geochemical comparisons

The geochemical compositions of the Archean rocks described in this work were compared with those reported in the Quadrilátero Ferrífero region by Farina et al. (2015). The authors suggested that these Archean terranes mainly constitute two geochemically distinct rock groups: (i) banded gneisses + plagioclase-rich granitoids (predominant between ca. 3200 and 2760 Ma) and (ii) K-feldspar-rich granites with lesser amounts of K-feldspar-bearing gneisses (prevailing from ca. 2760–2610 Ma). These groups plot in the fields of "medium-K" and "high-K" rocks in the SiO_2 vs. K_2O diagram, respectively (Fig. 7e). Part of the banded gneisses and plagioclase-rich granitoids of Farina et al. (2015) present slight geochemical variations from the typical TTG compositions of Moyen and Martin (2012), which precludes classifying these rocks as true TTGs.

The L1 Bt-poor tonalitic gneiss and the L2 granodioritic gneiss are similar to the "medium-K" banded gneisses and Plg-rich granitoids of Farina et al. (2015), while the L1 Bt-rich tonalitic gneiss, the Hbl-bearing tonalitic gneiss, and the xenoliths show lower SiO_2 and, to some extent, lower Na_2O, and enrichment in FeO_t + MgO, CaO, Rb and Rb/Sr (Figs. 7a–f and 13). The L2 granitic gneiss and the L4 metagranite plot in the field of the "high-K" granitic rocks of Farina et al. (2015; Figs. 7a–f and 13a and b). The Hbl-bearing granitic gneiss plots outside the fields of Farina et al. (2015), mostly concerning the K_2O, Na_2O, Rb, Rb/Sr and Sr/Y values (Figs. 7a–f and 13a and b). In the multi-element patterns, the L2 granodioritic gneiss and the Hbl-bearing tonalitic gneiss are similar to the medium-K banded gneiss (Figs. 8 and 9b). The L2 granitic gneiss and the L4 metagranite show overall the same pattern as the high-K gneisses and granites of Farina et al. (2015; Figs. 8 and 9c and d), except for the low LREE of L4.

Campos and Carneiro (2008) and Engler et al. (2002) also identified Archean rock types such as TTG, biotite and two-mica granites and sanukitoids in the Passa Tempo and Campo Belo complexes, although not all the rocks from the latter group can be undoubtedly classified as such. This conclusion is possibly due to the fact that a high proportion of the geochemically analyzed samples are hybrids, even if this terminology was not applied at the time. The L1 Bt-poor tonalitic gneiss geochemically fits the enderbitic rocks described in the Perdões region, Campo Belo Complex (Engler et al., 2002), and differs from the Aureliano Mourão trondhjemite of the Passa Tempo Complex (Campos and Carneiro, 2008) mainly in terms of Ba and Sr proportions, which are higher for this body. The L2 granitic gneiss is similar to part of the biotite and two-mica granites described by Campos and Carneiro (2008) in the Passa Tempo Complex, while the Hbl-bearing granitic gneiss is akin to the São Pedro da Carapuça granite of the same complex. The chemical composition of the Hbl-bearing tonalitic gneiss, especially regarding its Ba and Sr contents coupled with the high ferromagnesian oxides, has no Archean analogs in the entire southern São Francisco Craton.

5.2.2. Correlations with tectono-magmatic events of the southern São Francisco craton

Due to the scarcity of outcrops and older age compared with all the other lithotypes, we consider that the L1 Bt-rich tonalitic gneiss (2816 ± 30 Ma) constitutes xenoliths hosted by the São Tiago Batholith, which are representative of a Mesoarchean crust. In the context of the southern São Francisco Craton, the age of the L1 Bt-rich tonalitic gneiss roughly matches that of the Rio das Velhas II/Neoarchean 1 event (ca. 2800–2750 Ma), during which TTG plutons were emplaced in the Quadrilátero Ferrífero region, mainly in the Bonfim and Belo Horizonte complexes (Lana et al., 2013; Teixeira et al., 2017).

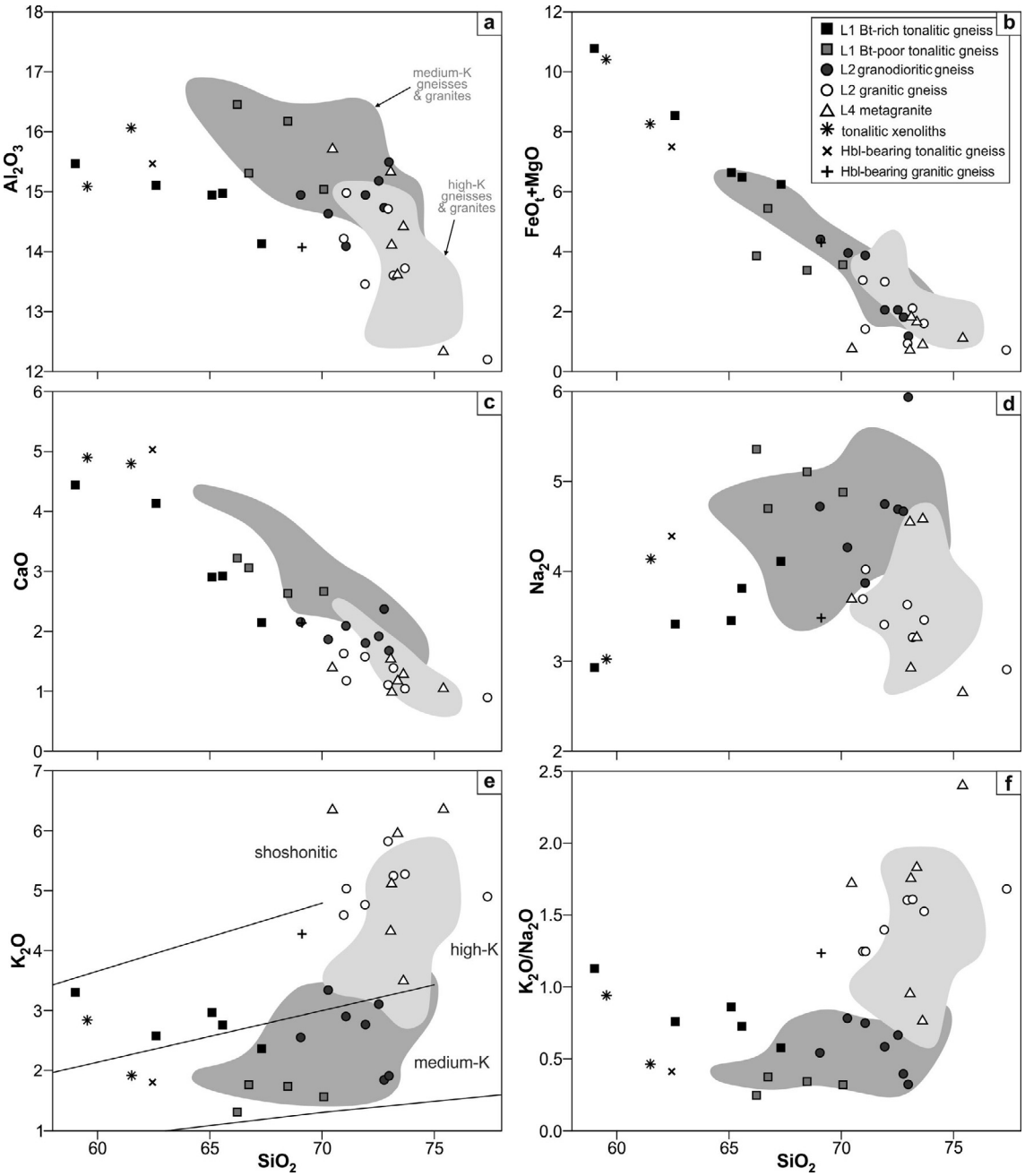

Fig. 7. Harker diagrams showing selected major oxides of the main lithotypes of the São Tiago orthogneiss and adjacent bodies. (a) Al_2O_3 vs. SiO_2; (b) FeO_t + MgO vs. SiO_2; (c) CaO vs. SiO_2; (d) Na_2O vs. SiO_2; (e) K_2O vs. SiO_2 with the fields of Peccerillo and Taylor (1976); (f) K_2O/Na_2O vs. SiO_2. The gray fields refer to medium-K (banded gneiss and plagioclase-rich granitoids) and high-K (K-feldspar-rich granite and K-felspar-bearing gneisses) rocks from the Quadrilátero Ferrífero region, to the NE of the study area. Data from Farina et al. (2015).

The time interval for the progressive replacement of TTG by potassic I-type granitic magmatism registered in the Quadrilátero Ferrífero extends from ca. 2780 to 2750 Ma (Romano et al., 2013), a transition that is documented worldwide in the age range of 3000–2500 Ma (Laurent et al., 2014). At the time of the Mamona event defined by Farina et al. (2015; 2760–2680 Ma) in the Quadrilátero Ferrífero, high-K plutons composed of granites, granodiorites and leucogranites were emplaced. In this sense, the crystallization ages of the L2 granitic gneiss (2664 ± 4 Ma) and the cogenetic L3 pegmatite (2657 ± 23 Ma) are interpreted here as contemporaneous with the main potassic magmatism of that region. The potassic magmatism lasted until ca. 2610 Ma (Romano et al., 2013), as recorded in a few plutons in the Quadrilátero Ferrífero, but some authors extend it to ca. 2550 Ma (Teixeira et al., 2017). In fact, Teixeira et al. (2017) incorporated the Neoarchean potassic magmatism in a major event of crustal reworking of the southern São Francisco Craton within the 2720–2550 Ma interval, which involved granulite-facies metamorphism and migmatization and emplacement of layered mafic-ultramafic intrusions. Although most of the migmatization superimposed both S_n and S_{n+1}, local partial melting enclosed by foliation planes and along the axial planes of S_{n+1} may suggest that those features are contemporaneous, related to a single deformational-metamorphic event that may had been responsible for S_n and S_{n+1} in the L2 and L3 lithotypes and for the migmatization of L2. However, it is still unclear if such event is correlated with Late Archean migmatization episodes that occurred in the southern São Francisco Craton at ca. 2660 and ca. 2600 Ma (Campos et al., 2003; Toledo et al., 2010).

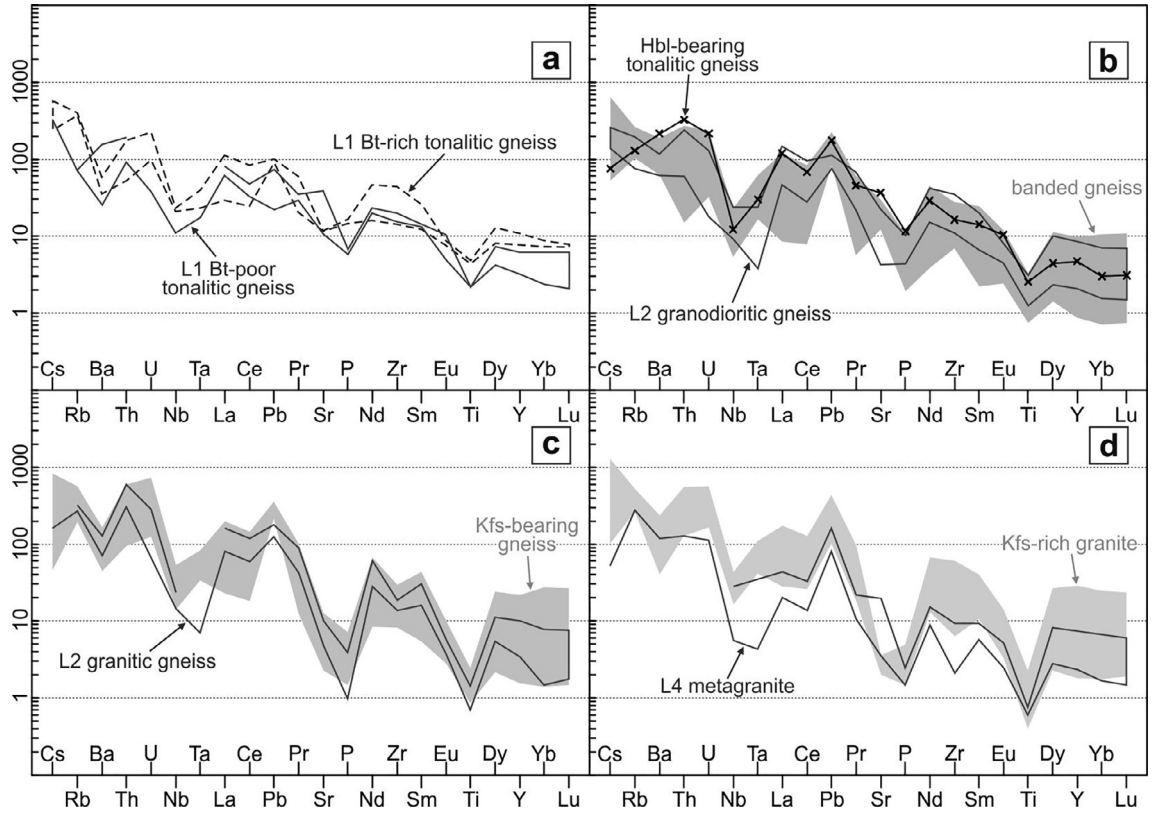

Fig. 8. Mantle-normalized multi-element diagram for rocks of the São Tiago Batholith and associated units. Gray fields for the banded and K-feldspar-bearing gneisses and K-feldspar-rich granite are from the Quadrilátero Ferrífero region, to the NE of the study area. Data from Farina et al. (2015). Primitive mantle after McDonough and Sun (1995).

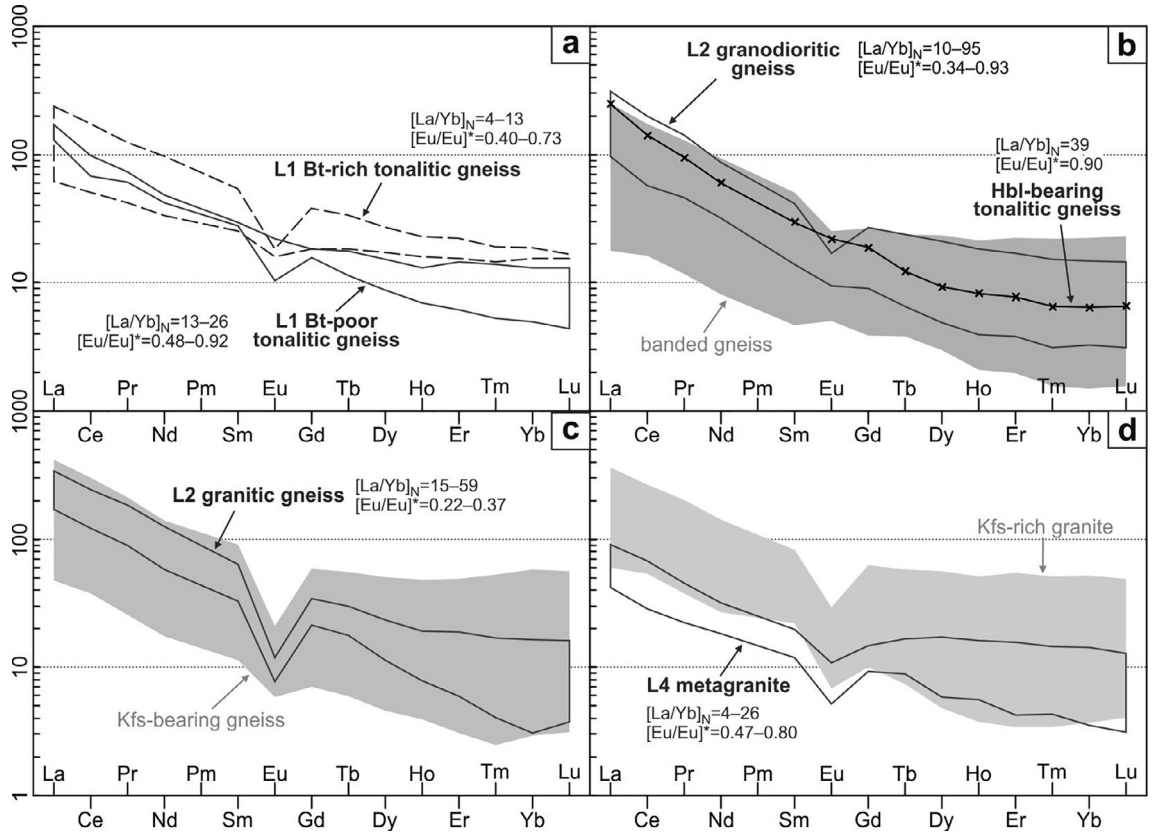

Fig. 9. Chondrite-normalized rare earth elements diagram for the studied rocks (chondrite values after Boynton, 1984). Gray fields for the banded and K-feldspar-bearing gneisses and K-feldspar-rich granite are from the Quadrilátero Ferrífero region, to the NE of the study area. Data from Farina et al. (2015).

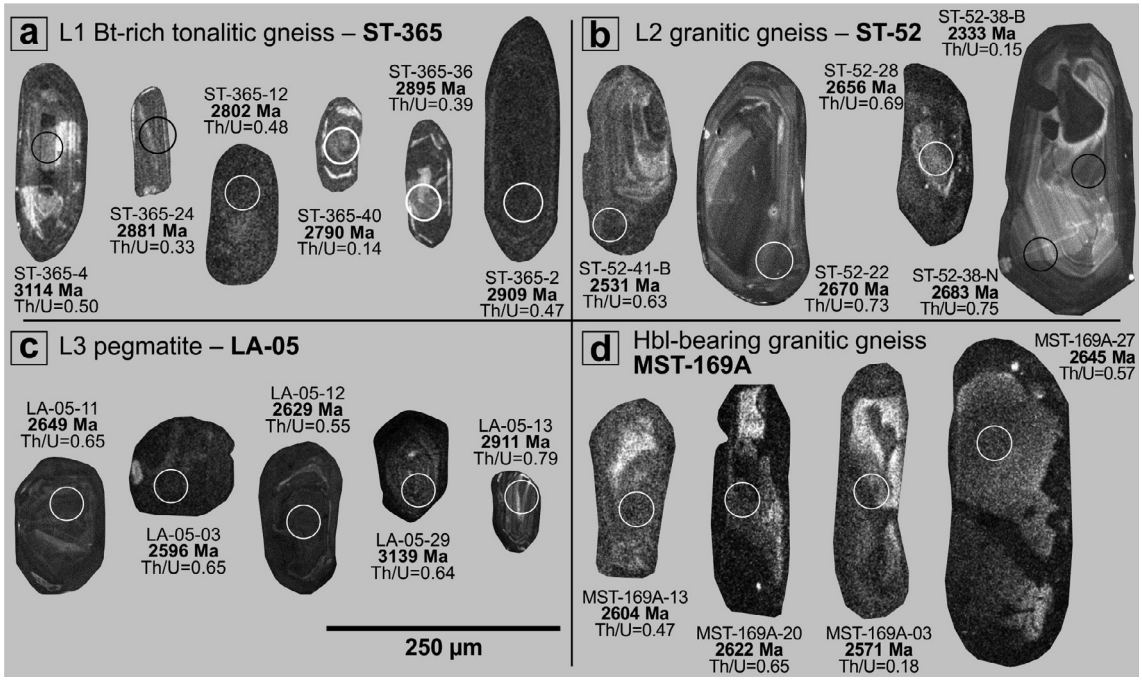

Fig. 10. Cathodoluminescence images of selected zircon grains used for age dating. The circles indicate the laser spots position where the $^{207}Pb/^{206}Pb$ ages were obtained. The scale is the same for all samples. See Fig. 1 for sample location.

The crystallization age of 2614 ± 13 Ma obtained for the Hbl-bearing granitic gneiss may be correlated to the youngest pulse of potassic magmatism registered in the southern São Francisco Craton ca. 2610 Ma (Romano et al., 2013). The gneissic foliation observed in this body, and previous descriptions of small bodies of foliated granodiorites crystallized at the same age (ca. 2612 Ma Romano et al., 2013) require a younger deformation episode. It may be associated with the late Neoarchean major event of crustal reworking, or with Paleoproterozoic docking of the Mineiro belt against the São Francisco Protocraton.

Our observations in the São Tiago region show that the Meso- to Neoarchean crust includes eight different metaigneous and gneissic rocks. The fact that all the obtained crystallization ages are Archean is at odds with the previous assumption of Silva et al. (2002) that the São Tiago Batholith is a Paleoproterozoic unit of the Mineiro belt. Toledo et al. (2010) attributed the obtained age of 2050 ± 12 Ma of Silva et al. (2002) to magmas generated by exhumation of the São Tiago Batholith in a dome-and-keel formation process. An alternative explanation could be that Silva's sample belongs to one of the Paleoproterozoic metagranitoids that surround the São Tiago Batholith. Furthermore, the presence of Neoproterozoic lower intercept ages and the absence of Paleoproterozoic ones may suggest that a possible Neoproterozoic overprint might have been stronger than a Paleoproterozoic one.

5.3. Petrogenetic interpretation

In the Quadrilátero Ferrífero region, Farina et al. (2015) proposed that the production of medium-K rocks results from mixing between magmas generated by partial melting of metamafic sources and older TTG rocks, whereas high-K granitoids are associated with partial melting of Archean metasedimentary rocks. In this sense, the compositional diversity among the eight lithotypes mapped in the São Tiago region reflects a wide spectrum of petrogenetic processes, Archean in age.

5.3.1. Origin of the L1 subtypes

The L1 Bt-rich tonalitic gneiss (2816 ± 30 Ma) is more mafic, shows higher K_2O, CaO, FeO_t + MgO and transitional metals (not shown), lower Na_2O, and relatively flatter REE patterns with stronger negative Eu anomalies than the L1 Bt-poor tonalitic gneiss. Discontinuous trends of K_2O vs. SiO_2 and Na_2O vs. SiO_2 (Fig. 7d and e) and contrasting Sr contents (Table 1) preclude fractional crystallization between the L1 subtypes.

The comparatively higher-silica L1 Bt-poor subtype carries geochemical characteristics of TTG magmas generated in medium- to low-pressure environments close to the upper limit of the plagioclase stability field (Fig. 12b). Indeed, high Na_2O, moderately high $[La/Yb]_N$ with slightly negative [Eu/Eu]* anomalies, and low K_2O/Na_2O and Y (Fig. 7d, f; Fig. 9; Table 1) contents suggest the melting of metabasalts leaving a clinopyroxene-, amphibole-, and plagioclase-rich residue with moderate to few garnet. Such generation process partially corresponds to both medium- and low-pressures TTG petrogeneses (Moyen, 2011). Additionally, the source basalts should be somewhat enriched, as pointed by Martin et al. (2014), since MORB-like basalts hardly generated TTG melts with K_2O > wt.1% on most partial melting experiments (cf. Fig. 14). The source should present higher LILE including 0.5 < K_2O < wt.1.2%, a feature exhibited by the average-Archean basalt (Martin et al., 2014). Retaining of titanite, ilmenite or rutile in the source is also suggested by the negative Ti, Nb, and Ta anomalies (Fig. 8).

The high ferromagnesian elements and transitional metals, as well as high calcium suggest a mafic melting source for the L1 Bt-rich tonalitic gneiss (Fig. 14). However, either that source had been previously K_2O-enriched, or the mafic original melt had suffered contamination of a crustal component, due to high potassium contents of the gneiss. In the literature, the rare experimental and modeled melts which present the composition of the L1 Bt-rich tonalitic gneiss have high-K andesitic sources (Alonso-Perez et al., 2009; Beard and Lofgren, 1991), but the melts remain too poor in K_2O, which favors the contamination hypothesis. On the other hand, its internal variability could not be related with increasing degrees of contamination of a K_2O- and SiO_2-enriched end-member, since the potassium has negative linear correlation with silica. Decreasing K_2O and increasing Na_2O, HFSE and Y towards the more felsic pole may point to differentiation of the L1 Bt-rich tonalitic gneiss, possibly related with biotite fractionation.

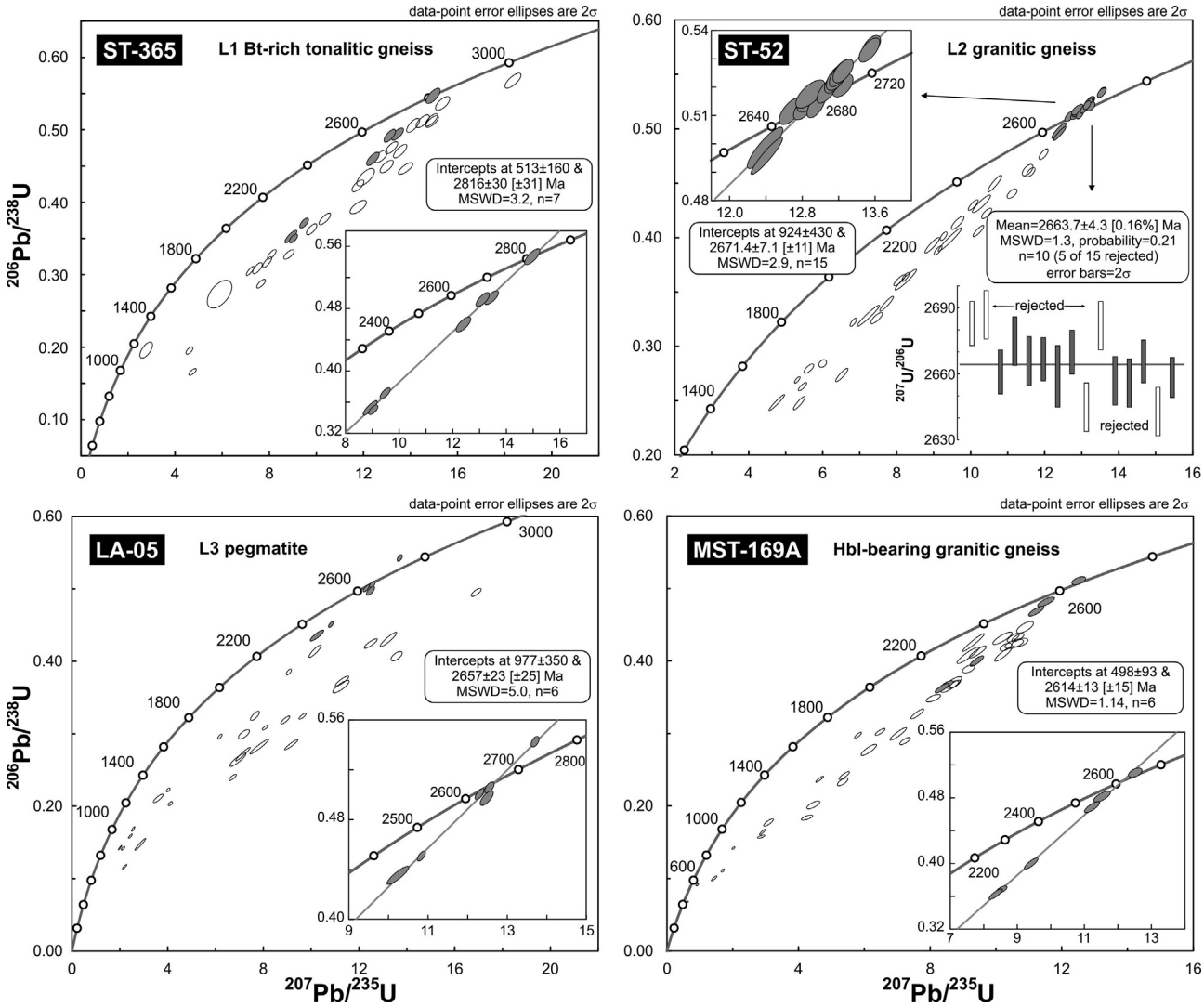

Fig. 11. U–Pb concordia diagrams of LA-ICP-MS analyses on zircon crystals of the São Tiago Batholith and associated units. See Fig. 1 for sample location.

5.3.2. Origin of the L2 subtypes

The L2 granitic gneiss is high-K and medium-Na, whereas the L2 granodioritic gneiss is medium-K and high-Na (Fig. 7d and e). Considering trace element data, the L2 granitic gneiss has stronger [Eu/Eu]* anomalies (Fig. 9), higher Rb and Rb/Sr, and lower Sr/Y vs. SiO_2 (Fig. 13) in comparison with the L2 granodioritic gneiss. Based on these characteristics, the L2 subtypes are not considered cogenetic, and their genesis is treated separately hereafter.

The slightly enrichment in Na_2O and the reduction in K_2O of the L2 granodioritic gneiss relative to the L1 Bt-poor tonalitic gneiss may suggest that the latter may be a viable melting source to generate the former. The similarity also suggests high degrees of partial melting of TTG or TTG-like rocks, which would promote the incipient enrichment of K_2O, the more pronounced negative Nb and Ta anomalies, and the negative Eu anomalies associated with retaining of ilmenite-rutile, amphibole, and plagioclase in the source. Alternatively, in terms of major oxides data, the L2 granodioritic gneiss is quite similar to the melts derived from experimental partial melting of quartz amphibolite in the highest pressure conditions (15 kbar; Patiño-Douce and Beard, 1995). It worth noting that the two possible sources (the L1 Bt-poor tonalitic gneiss and a quartz amphibolite) present intermediary to felsic composition with K_2O between 0.7 and 1.6 wt%.

The L2 granitic gneiss (2664 ± 4 Ma) is compositionally similar to Late Archean "biotite and two-mica granites". Laurent et al. (2014) proposed that these compositions could be derived from partial melting of two distinct crustal sources: TTGs or metasedimentary rocks. Most melting experiments on medium-K felsic rocks such as L1 Bt-poor tonalitic gneiss produced melts which are mostly depleted in K_2O and enriched in Na_2O, even in the best match provided by Watkins et al (2007) using a hornblende-bearing tonalitic gneiss source (cf. Fig. 14). The enrichment in LILE and LREE, and depletion in Sr, Ti, Nb, and Ta of this gneiss suggest that L1 Bt-rich tonalitic gneiss may be a viable source for melting. Additionally, the composition of the melts generated by the experiment of Patiño-Douce (2005), whose source is overall similar with the L1 Bt-rich tonalitic gneiss, are geochemically akin to the L2 granitic gneiss. The only difference is the higher Al_2O_3 of the melts, which may reflect the enrichment on the same oxide in the source. The match is more accurate under higher pressure conditions (27–32 kbar). Other experiments show that dehydration melting of metagraywackes (cf. Montel and Vielzeuf, 1997), such those from the coeval Rio das Velhas greenstone belt, could contribute additional K_2O to the compositions of the produced melt. The petrographic and geochemical differences among samples of the L2 K-rich granitic gneiss (e.g., variable microcline/plagioclase and K_2O/Na_2O proportions) would then be associated with a variable melting proportion of metasedimentary rocks. Then, the L2 granitic gneiss should have been generated by the melting of the L1 Bt-rich gneiss and/or by the melting of a metasedimentary/TTG mixed source.

Table 2
Summary of petrological and geochronological characteristics of the studied gneisses and metagranites from the São Tiago region, including comparison with selected rocks of the Quadrilátero Ferrífero (Farina et al., 2015). (a) Geochronological data of the São Tiago region are from this work and of Quadrilátero Ferrífero from Farina et al. (2015); (b) When one or two values of determined parameter are considerably distant of the remnant values, the median is indicated inside the bracket after the full range of values [e.g., 1–42 (2)]; (c) Normative classification based on the CIPW norm plotted in the Ab-Na-Or diagram of O'Connor (1965) with the fields of Barker (1979): *grd* = granodiorite; *tdj* = trondhjemite; *gr* = granite; *to* = tonalite.

	Rocks of São Tiago region (this work)						
	São Tiago orthogneiss				xenoliths into São Tiago orthogneiss		
	L2		L3	L4	L1		tonalitic xenoliths
	granodioritic gneiss	*granitic gneiss*	*pegmatite*	*metagranite*	*Bt-rich tonalitic gneiss*	*Bt-poor tonalitic gneiss*	
U-Pb crystallization age (Ma) (a)		*2664 ± 4*	*2657 ± 23*		*2816 ± 30*		
Geochemical data (b)							
SiO_2	69.1–73.0	71.1–77.3	No obtained data	70.5–75.4	59.0–67.3	66.2–70.1	59.5–61.5
Al_2O_3	14.1–15.5	12.2–14.7		12.3–15.7	14.1–15.5	15.0–16.5	15.1–16.1
FeO_t + MgO	1.2–4.8	0.8–3.3		0.8–2.0	6.8–11.6	3.6–5.9	8.8–11.2
CaO	1.7–2.4	0.9–1.6		1.0–1.5	2.1–4.4	2.6–3.2	4.8–4.9
Na_2O	3.9–5.9	2.9–4.0		2.7–4.6	2.9–4.1	4.7–5.4	3.0–4.1
K_2O	1.8–3.3	4.6–5.8		3.5–6.4	2.4–3.3	1.3–1.8	1.9–2.8
K_2O/Na_2O	0.32–0.78	1.24–1.68		0.76–2.40	0.72–1.35	0.24–0.37	0.46–0.94
Norm. class. (c)	*tdj/gr*	*gr*		*gr*	*grd*	*tdj*	*to/grd*
V	7–55	6–32		10–19	62–85	30–48	75–88
Ni	2–40 (9)	2–5		1–42 (2)	11–45	4–15	44–48
Ba	179–822	464–841		605–1094	234–383	232–1024	180–673
Rb	45–213	165–196		139–218	174–243	43–142	113–184
Sr	84–451	95–196		70–466	123–253	214–778	228–301
Y	8–37	11–43		10–32	26–75	14–27	24–28
Sr/Y	2.30–49.89	2.63–13.61		2.11–19.50	2.15–9.81	10.59–29.35	8.11–12.54
Sr/Ba	0.11–2.03	0.14–0.27		0.09–0.65	0.61–1.02	0.76–1.29	0.45–1.27
REE systematics	Low to high fraction $[La/Yb]_N$ = 10–95 [Eu/Eu]* = 0.34–0.93	Med/high fraction $[La/Yb]_N$ = 15–59 [Eu/Eu]* = 0.22–0.37		Low/med fraction $[La/Yb]_N$ = 4–26 [Eu/Eu]* = 0.47–0.80	Low fraction $[La/Yb]_N$ = 4–13 [Eu/Eu]* = 0.40–0.73	Med fraction $[La/Yb]_N$ = 13–26 ([Eu/Eu]* = 0.48–0.92	

	Rocks of São Tiago region (this work)		Rocks from Quadrilátero Ferrífero (Farina et al., 2015)			
	other bodies		banded gneiss	Plg-rich granitoids	Kfs-bearing gneiss	Kfs-rich granite
	Hbl-bearing tonalitic gneiss	Hbl-bearing granitic gneiss				
U-Pb crystallization age (Ma) (a)		*2614 ± 13*	ca. 3200–2760	ca. 2790–2680	2854 ± 18, 2764 ± 10	ca. 2760–2680; ca. 2610
Geochemical data (b)						
SiO_2	62.4	69.1	64.7–74.4	68.0–73.9	70.8–75.8	72.3–75.3
Al_2O_3	15.5	14.1	13.9–16.7	14.1–15.4	12.7–15.0	12.6–13.9
FeO_t + MgO	8.0	4.7	1.6–6.9	1.6–5.6	1.9–3.9	1.1–5.0
CaO	5.0	2.1	1.5–4.3	1.4–3.9	0.7–2.5	0.9–1.6
Na_2O	4.4	3.5	4.3–5.5	3.4–5.0 (4.6)	3.4–4.7	2.7–3.8
K_2O	1.8	4.3	1.6–3.5	2.3–3.0	2.9–4.9	4.7–5.7
K_2O/Na_2O	0.41	1.23	0.32–0.81	0.53–0.74	0.63–1.44	1.22–1.91
Norm. class. (c)	*to*	*gr*	*gr/tdj/grd*	*gr/tdj/grd*	*tdj/gr*	*gr*
V	87	43	22–86	18–75	22–39	12–25
Ni	42	8	6–27	6–16	5–10	5–13
Ba	1422	848	420–1258	288–1015	335–1101	263–1547
Rb	78	210	61–158	69–145	116–343	156–317
Sr	728	153	240–602	138–440	59–251	45–70
Y	20	73	4–42	6–45	7–93	8–125
Sr/Y	36.22	2.10	5.69–134.64	3.44–68.00	0.49–37.36	0.53–9.02
Sr/Ba	0.51	0.18	0.20–0.99	0.26–0.60	0.14–0.52	0.04–0.18
REE systematics	High fraction. $[La/Yb]_N$ = 39 [Eu/Eu]* = 0.90		Low to high fraction $[La/Yb]_N$ = 4–49 (17) [Eu/Eu]* = 0.67–1.31	Low to high fraction $[La/Yb]_N$ = 9–51 [Eu/Eu]* = 0.33–1.26	Low/med fraction $[La/Yb]_N$ = 5–21 (12) [Eu/Eu]* = 0.13–0.80	Low/med fraction $[La/Yb]_N$ = 3–21 (7) [Eu/Eu]* = 0.19–0.50

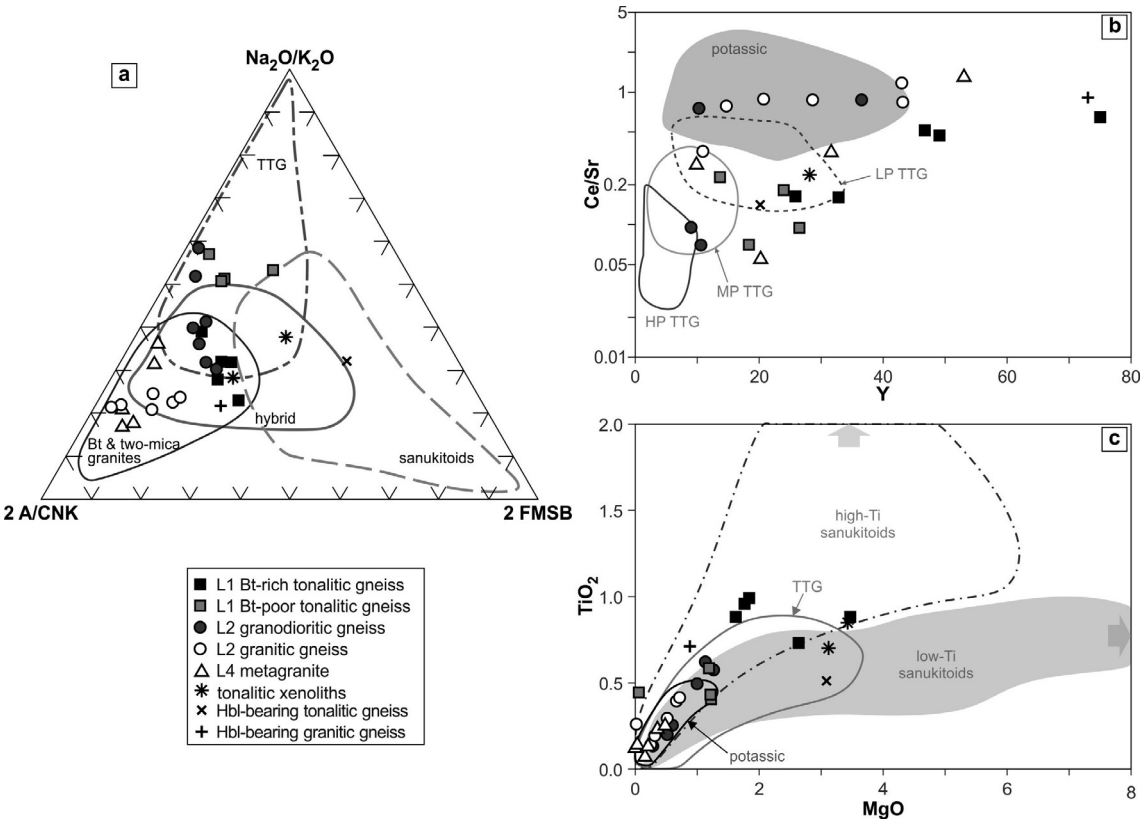

Fig. 12. (a) Geochemical discrimination diagram for late Archean granitoids proposed by Laurent et al. (2014). Variables are: 2*A/CNK (= molar Al_2O_3/[CaO + Na_2O + K_2O] ratio); Na_2O/K_2O ratio; 2*FMSB (= [2*(FeO_t + MgO)wt% * (Sr + Ba)wt%]). (b) Ce/Sr vs. Y discrimination diagram of Moyen (2011) for the three types of TTG and potassic rocks that compose the Archean gray gneisses (HP – high-pressure; MP – medium-pressure, LP – low-pressure). (c) Diagram modified after Martin et al. (2009), for the high-Ti and low-Ti sanukitoids; additional fields for TTG and potassic rocks data are from Moyen (2011).

5.3.3. Origin of the L4 lithotype

The L4 metagranites comprise heterogeneous samples but are geochemically similar to the L2 K-rich granitic gneiss. The strong variation of K_2O and Y and the lack of clear correlation trends among L4 samples, however, suggest multiple origins. Slightly peraluminous, potassic and calc-alkaline biotite-bearing Archean granites are described as a result of partial melting of older felsic crust, mainly TTGs (Almeida et al., 2013; Frost et al., 2006; Moyen et al., 2003; Sylvester, 1994; Whalen et al., 2004). Again, a metasedimentary source may have an important role on the genesis; the great variations in K_2O and Na_2O in the L4 group may reflect a mixed TTG-sedimentary source, and higher the sedimentary component, higher the K_2O/Na_2O ratio. Thus, strong negative P and Ti anomalies (Fig. 8) and low $[La/Yb]_N$ and Sr/Y (Figs. 9 and 13c) imply a garnet-free and plagioclase-apatite-titanite-ilmenite-rich melting residue.

5.3.4. Origin of Hbl-bearing tonalitic and Hbl-bearing granitic gneisses

Since only single samples of both Hbl-bearing tonalitic and granitic gneisses were geochemically analyzed, their investigation was performed only for purposes of comparison, and only general petrogenetic processes are suggested here.

The metaluminous Hbl-bearing tonalitic gneiss shows high CaO (5%), FeO_t + MgO (8%), Mg# (53) and transitional metal (V and Cr) values and low K_2O/Na_2O (0.41), which suggest the involvement of melts derived from mantle peridotite. However, the high contents of LILE, especially Ba and Sr (Ba > 1000, Sr > 500) and light REE, as well as moderate Th and U, imply melting of previously metasomatized mantle. In fact, the geochemistry of the Hbl-bearing tonalitic gneiss is similar to typical sanukitoid s.l. of Heilimo et al. (2010).

The Hbl-bearing granitic gneiss (2614 ± 13 Ma) exhibits most of the characteristics of the "biotite and two-mica" granites of Laurent et al. (2014) but with considerably higher hornblende contents and relatively high CaO (> 2%), FeO_t + MgO (> 4%), V (> 40 ppm), and Zr (> 300 ppm). These values are typical of "high-Ti sanukitoids" (Martin et al., 2009; Fig. 13c). Therefore, the features of the hornblende-bearing monzogranitic gneiss are concordant with "hybrid" granitoids (Laurent et al., 2014) and could have resulted from the interaction between felsic sanukitoids and crustal melts.

5.4. Geotectonic implications

The literature regarding the tectonic scenario of the southern São Francisco Craton in the Neoarchean indicates the existence of an active continental margin, including events of subduction, collision, and crustal reworking, until the Minas passive margin stage developed (Campos and Carneiro, 2008; Farina et al., 2016; Goulart et al., 2013; Moreira et al., 2016; Teixeira et al., 2017). Martínez Dopico et al. (2017) summarized the geodynamic evolution of the Quadrilátero Ferrífero during 2800–2600 Ma as follows:

(i) ca. 2800 Ma – Paleoarchean and Mesoarchean crust are reworked, and arc type magmas (mainly TTGs and TTG-like with minor mafic melts) are produced in a subduction environment. At this time, the Rio das Velhas Basin, including Rio das Velhas II magmatism of the Nova Lima group, is developed.
(ii) ca. 2750 Ma – Collision and uplift of older crust, reactivation of previous suture zones, and changes in mechanisms and sources of magma production occur, (i.e., Mamona potassic magmatism; 2760–2680 Ma; Farina et al., 2015); Maquiné basin develops (Moreira et al., 2016).
(iii) ca. 2700 Ma – Orogenic collapse and post-collisional magmatism occur, the Mamona event reaches its peak, and the Caraça Group

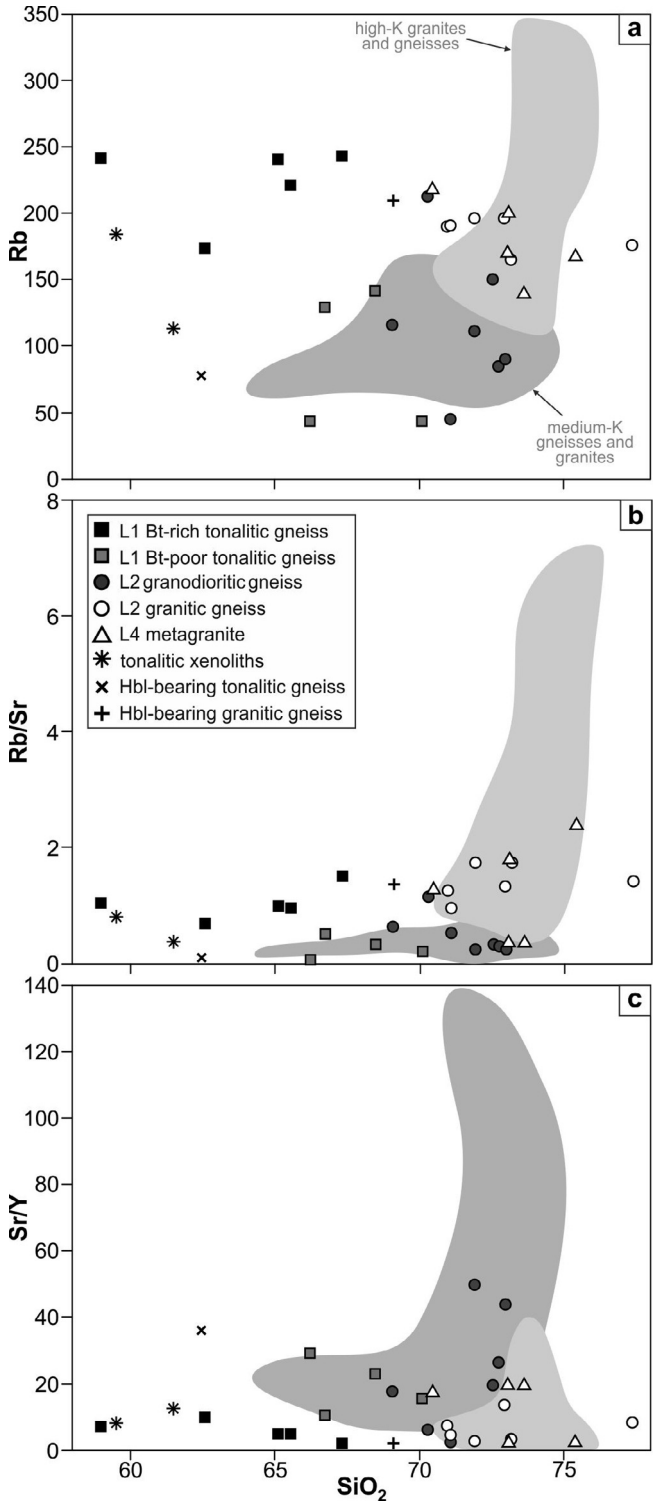

Fig. 13. Harker diagrams showing selected trace elements of the main lithotypes of the São Tiago orthogneisses and metagranites, and the other studied gneisses. (a) Rb vs. SiO_2; (b) Rb/Sr vs. SiO_2; (c) Sr/Y SiO_2. The gray fields refer to medium-K (banded gneiss and plagioclase-rich granitoids) and high-K (K-feldspar-rich granite and K-felspar-bearing gneisses) rocks from the Quadrilátero Ferrífero region. Data from Farina et al. (2015).

starts to be deposited in a continental near-shore environment.

(iv) ca. 2600 Ma – The Minas passive margin stage begins, as well as the final potassic magmatism.

Campos and Carneiro (2008) considered two main Neoarchean events of granitoid genesis in the Campo Belo and Passa Tempo complexes: one related to TTG magmatism in an environment of subducting basaltic oceanic crust and the other to partial melting of the preexisting continental crust, generating the potassic granites of the region. Such reworking included a dextral, transpressive, ductile-brittle regime, with the surface of flow and tectonic transport from NE to SW (Campos et al., 2003; Campos and Carneiro, 2008), coherent with the major event of crustal reworking of the southern São Francisco Craton (Teixeira et al., 2017).

The evolution of the Archean São Tiago Batholith is complex and involves diverse rock types. The early crust formed in the São Tiago region is represented by the L1 lithotype of Mesoarchean age (2816 ± 30 Ma). We advocate that partial melting of a basaltic oceanic crust transformed into garnet-bearing amphibolite at medium to low pressures could produce the L1 Bt-poor tonalitic gneiss protolith (Fig. 15a). In the literature about TTG petrogenesis, many authors have claimed an origin related with melting of the base of much thickened oceanic plateaus, whose composition and pressure–temperature conditions would be coherent with melting of Ar-basalts (Martin et al., 2014) on sufficiently high pressure conditions (e.g., Smithies, 2000; Condie, 2005). However, low felsic magmas productivity on modern analogues, and the requirement of incredible high thickness to achieve the necessary pressure conditions, together with other isotopic evidences, led Martin et al. (2014) to suggest that TTG may have been generated by melting of subducting oceanic plateaus. The composition of the L1 Bt-poor tonalitic gneiss, however, points to an environment whose pressure is lower than most medium- and high-pressure TTG (i.e., TTG s.s.; Moyen, 2011; Moyen and Martin, 2012). We suggest that the L1 Bt-poor group may have been generated either by (i) partial melting of the base of an obducting, overthickened oceanic plateau (> 40 km), whose thickness is coherent with the one proposed for Archean oceanic plateaus (Kent et al., 1996; Nair and Chacko, 2008), or by (ii) partial melting of a subducting slab with great thickness but similar to today oceanic plateaus (20–30 km), in shallower conditions than the model of Martin et al. (2014; Fig. 15a). The second possibility is only partially analogous to the proposals of Lana et al. (2013) for TTG generation in the Quadrilátero Ferrífero, and of Campos and Carneiro (2008) for the TTG-like rocks of the Passa Tempo and Campo Belo complexes, since those two proposals did not mentioned the thickness of the subducting slab or pressure conditions. Both of our models differ from the genesis proposed for the enderbites from the Campo Belo Complex (Engler et al., 2002), related with melting of MORB in an undefined environment. Alternatively, Farina et al (2015) suggested a mixing origin between subduction and crustal reworking for the medium-K magmas of the Quadrilátero Ferrífero, especially those without clear TTG-signature (e.g., more potassic with negative Eu anomalies). Although the age of the L1 Bt-poor tonalitic gneiss was not obtained, we believe that it should be contemporary or most possibly younger than the L1-Bt-rich tonalitic gneiss, but definitively older than L2. The high proportion of compatible elements of the L1 Bt-rich gneiss points to original mafic magmas that have undergone crustal contamination, either by felsic rocks/magmas or sedimentary rocks. Many environments could be possible, including the subduction environment where L1 Bt-poor formed, and then we did not decided for a specific one.

After the end of the subduction of the oceanic crust and continental amalgamation (Fig. 15b) by ca. 2660 Ma, crustal thickening/collision promoted the generation of the L2, and L4 magmas. This process involved high-degree melting of the former TTG crust which is akin to the L1 Bt poor tonalitic gneiss (i.e., the L2 granodiorites), and melting of L1 Bt-rich gneiss and TTG/metasedimentary mixed sources related with the Rio das Velhas successions (i.e., the L2 granite, and the L4 granite). The deformational-metamorphic event which was responsible for the gneissic banding S_n transposed by S_{n+1} in the L2 and L3 lithotypes of the São Tiago Batholith and for the migmatization of L2 may had occurred at ca. 2660 Ma. If so, such event is correlated with Neoarchean

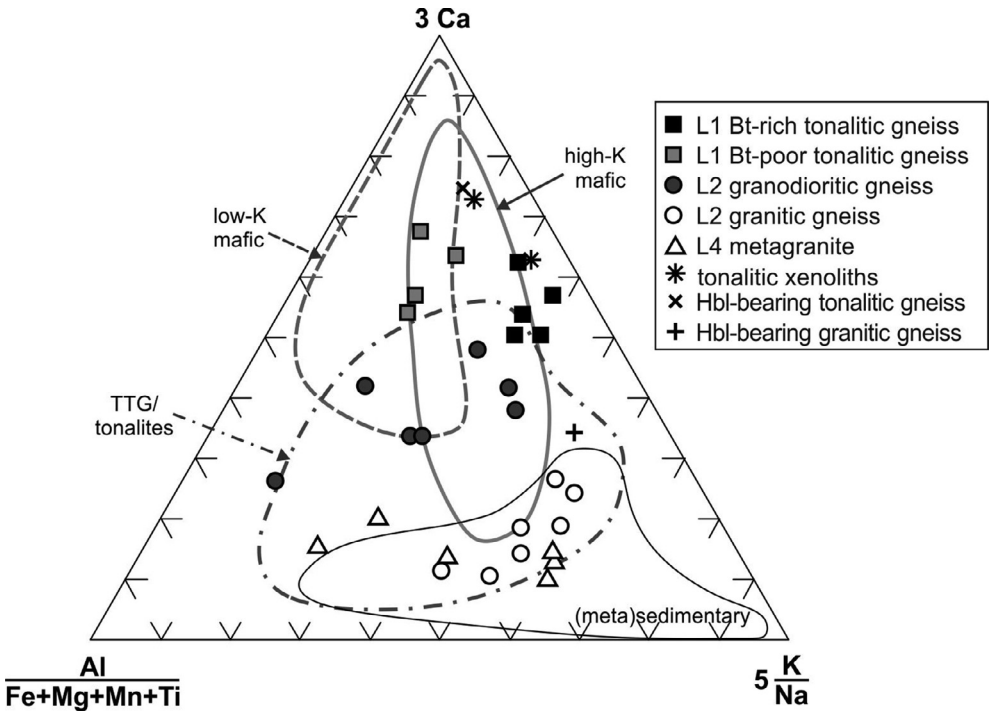

Fig. 14. Ternary diagram with molecular proportions of the elements after Laurent et al. (2014) for discrimination between potential source rocks for the meta-granitoids and gneisses of the São Tiago area. The 3Ca pole detects mafic sources; Al/(Fe + Mg + Mn + Ti) stands for felsic, crustal ones; and 5 K/Na tracks sedimentary sources. Fields were drawn using experimental melts of selected authors (consult Supplementary data 2 for the complete list of references).

migmatization episodes of the major crustal reworking event described by Teixeira et al. (2017) within the 2720–2550 Ma interval. The existence in the Passa Tempo Complex of mafic-ultramafic layered intrusions into the lower crust during this time interval corroborates the hypothesis of a thickened continental crust now exposed as a deeply eroded root zone (Teixeira et al., 2017). After this event of crustal production and reworking, the continental crust stabilized at least at 2650 Ma.

The last Archean magmatic pulse in the southern São Francisco Craton recorded in this work corresponds to the emplacement of the protolith of the hybrid hornblende-bearing monzogranitic gneiss (2614 ± 13 Ma), whose magmas were probably linked to the interaction between sanukitoid and crustal-derived melts in the continental crust. Those rocks may have been emplaced in an environment where the mantle-derived sanukitoid melts could interact with the felsic crust. Whether the sanukitoid magmas are related with the Hbl-bearing tonalitic gneiss or not primarily require the dating of this lithotype.

5.4.1. Late Archean to Paleoproterozoic evolution

The metavolcanic-sedimentary successions of the Minas Supergroup encircle the São Tiago Batholith to the south of the Jeceaba-Bom Sucesso lineament (Figs. 1 and 2). They are encompassed by Archean and/or Paleoproterozoic supracrustal successions intruded by Late Paleoproterozoic plutons of the Mineiro belt. There are three possible scenarios for this spatial configuration:

(i) The São Tiago Batholith and associated Neoarchean rocks may represent a peninsular portion of the Archean São Francisco Proto-craton, which was partially isolated from the rest of the craton by a shallow, narrow marine environment during the Archean–Paleoproterozoic transition at the time of deposition of the Minas Supergroup (Fig. 16a). An extensional regime was occurring, and the paleo-coastline for deposition of the Minas Supergroup would be represented by the Archean areas to the west of the Jeceaba-Bom Sucesso lineament). During the Early Paleoproterozoic, however, a compressive regime took over, with the first Paleoproterozoic arc-derived crust associated with the Minas accretionary orogeny (Fig. 16b; Teixeira et al., 2015). At this time, the paleo-coastline was marked by outcrops of the Minas Supergroup successions along the Jeceaba-Bom Sucesso lineament (JBL) to the south and east of the São Tiago Batholith, with a Paleoproterozoic sea bounding them (Fig. 16b).

(ii) The São Tiago region could represent in independent micro-terrane which amalgamated to the São Francisco Proto-craton only after the deposition of the Minas Supergroup, i.e., during the early stages of the Mineiro belt. In that case, the deformation associated with the continental collision should be the main gneissic foliation (S_n) into the São Tiago Batholith and essentially Paleoproterozoic. There is no conclusive evidence that corroborated that hypothesis.

(iii) The São Tiago Batholith could locally reproduce the regional-scale, dome-and-keel structures developed in the Quadrilátero Ferrífero area. The framework comprises crustal metamorphic nuclei partially or entirely outlined by Archean (i.e., Rio das Velhas greenstone) and Archean-Paleoproterozoic supracrustals (i.e., Minas Supergroup). This process is explained by the load shedding caused by orogenic collapse and the density differences between the hotter and lighter continental crust and colder and denser supracrustals (Marshak et al., 1992, 1997). Adjacent to the dome borders, high-temperature-low-pressure aureole-like bands (Jordt-Evangelista et al., 1992) result from the doming process in the Quadrilátero Ferrífero during the Paleoproterozoic (Sm-Nd determinations in garnet; Brueckner et al., 2000). We do not report metamorphic aureole-like minerals in supracrustal rocks surrounding the São Tiago Batholith. Moreover, contact metamorphism associated with the Paleoproterozoic Tabuões granitoid registered in the Minas succession along the Jeceaba-Bom Sucesso lineament (Neri et al., 2013; Quéméneur, 1987) brings additional difficulties for recognition of dome emplacement in the study area.

Although the “peninsula” and “micro-terrane” hypotheses are exclusive, the doming structure is not conflicting with those two former possibilities. They could rather have been consecutive, since either (i) the paleo oceanic floor in the case of the São Tiago crust isolated by a narrow sea or (ii) the suture area that resulted from amalgamation include rocks with greater density are more susceptible to sink during the load shedding.

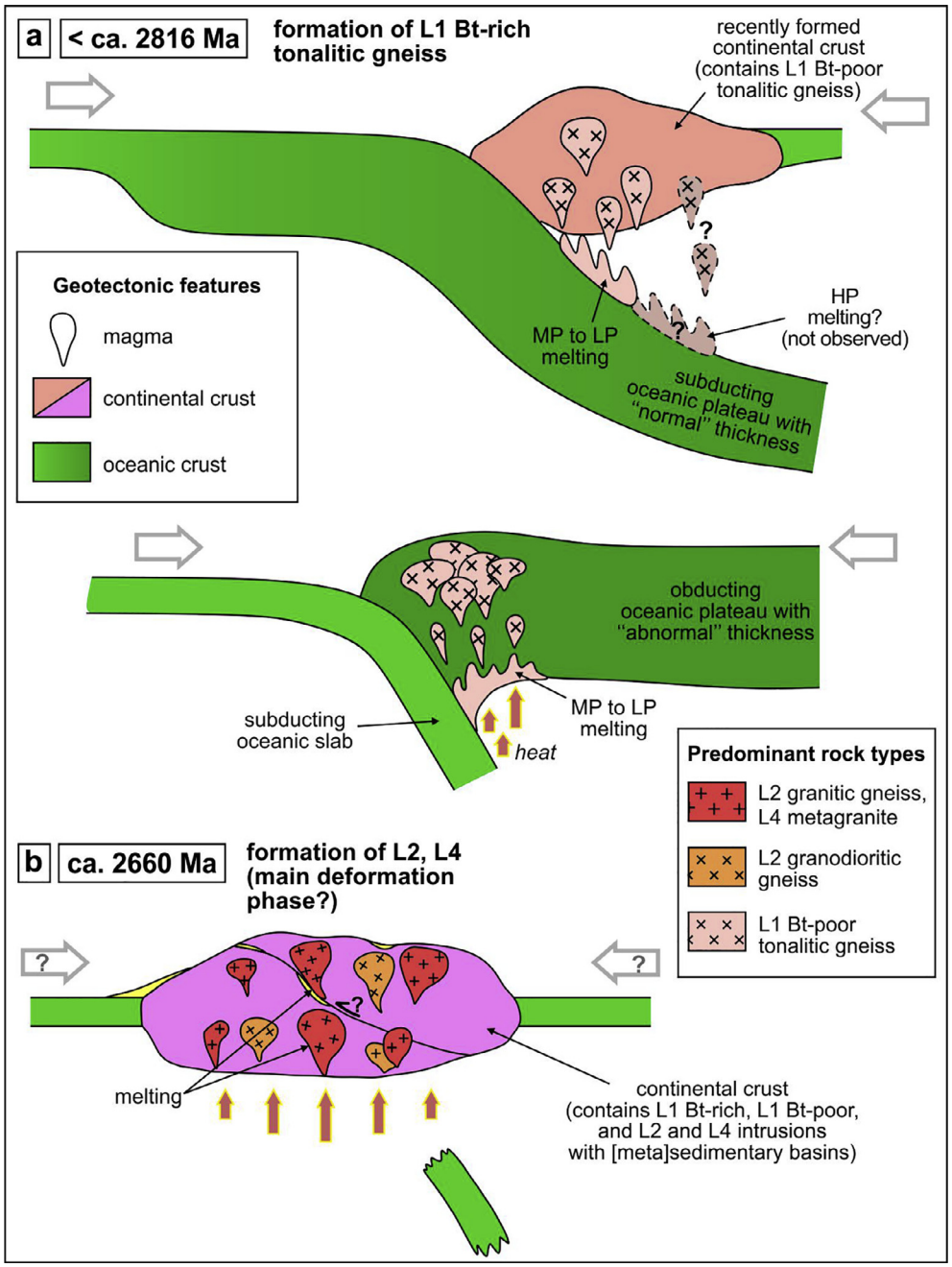

Fig. 15. Schematic cartoon for the Archean geotectonic evolution of the L1-Bt-poor tonalitic gneiss, the L2 granitic and granodioritic gneisses, and the L4 metagranite. (a) At 2816 Ma or later, the L1 Bt-poor tonalitic magmas may have been generated at low- to medium-pressures by partial melting of LILE-enriched mafic crust, either the base of an obducting overthickened oceanic plateaus, or a subducting normal oceanic plateau. (b) At the Neoarchean (ca. 2660 Ma), the predominant lithotypes of the São Tiago Batholith, L2 and L4, were generated. Our model suggests a Neoarchean agglutination leading to crustal thickening while the L2 and L4 magmas were generated. The L2 granodioritic magmas could be associated with partial melting of the former TTG crust, while TTG/metasedimentary mixed source or the L1 Bt-rich tonalitic gneiss could have produced via partial melting the protoliths of the L2 granitic gneiss, and the L4 metagranite.

6. Summary and conclusions

Fieldwork, petrography, geochemistry and geochronology for the São Tiago Batholith and coeval rocks defined an Archean domain close to the southern boundary of the Jeceaba-Bom Sucesso lineament, encompassed by Paleoproterozoic rocks of the Mineiro belt. The geochemical and geochronological investigations supported the following petrogenetic inferences and related tectonic settings for the studied lithotypes through time:

1) The L1 Bt-rich tonalitic gneiss (2816 ± 30 Ma) represents the oldest crustal component identified so far in the São Tiago region. Geochemical evidence suggests that the protolith of this lithotype originated by contamination of mafic magmas by crustal components in an unknown geotectonic scenario. The L1 Bt-poor tonalitic gneiss, with probably similar age, exhibit TTG affinity, and was generated at low- to medium-pressures by partial melting of LILE-enriched mafic lithologies of oceanic plateaus, either obducting overthickened or subducting normal ones in relatively shallow environments.. The age and geodynamic scenario of L1 correlate to the Rio das Velhas II/Neoarchean 1 event (ca. 2800–2750 Ma; Lana et al., 2013; Teixeira et al., 2017).
2) Neoarchean lithotypes of the São Tiago Batholith, which predominate in the main body, are the L2 granodioritic gneiss, the L2 granitic gneiss (2664 ± 4 Ma), the L3 pegmatite (2657 ± 23 Ma), and the L4 metagranite, which are mostly potassic rocks likely generated in a collisional environment. Our model suggests a Neoarchean agglutination leading to crustal thickening while the L2, L3, and L4 magmas were generated. In this regard, the protolith of the L2 granodioritic gneiss could be associated with partial melting of the former TTG crust. TTG/metasedimentary mixed source or the L1 Bt-rich tonalitic gneiss could had produced via partial melting the protoliths of the L2 granitic gneiss, and the L4 metagranite.

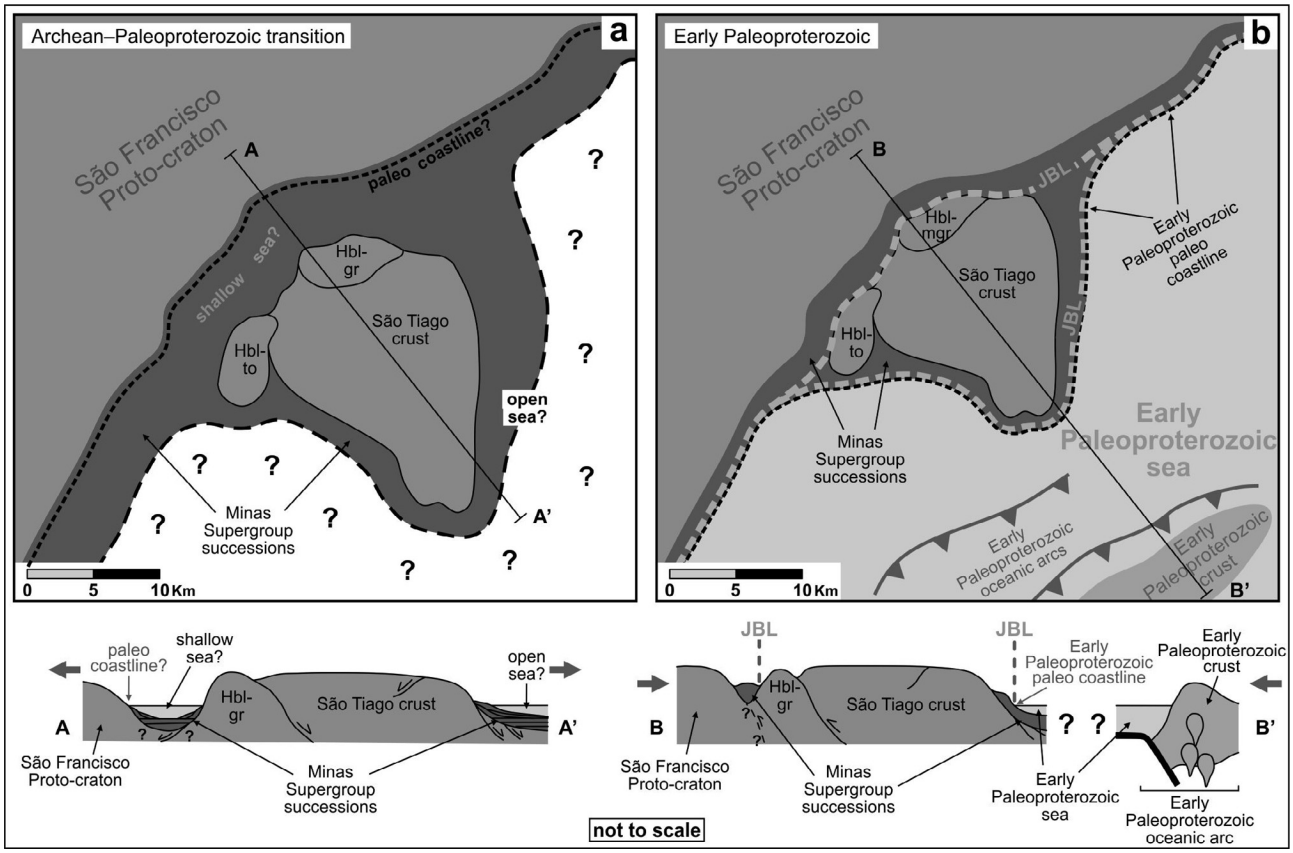

Fig. 16. Suggested reconstruction of the São Tiago crust during the Archean–Paleoproterozoic transition. (a) During the Archean–Paleoproterozoic transition, the São Tiago crust and the Hbl-bearing tonalitic (*hbl-to*) and granitic (*hbl-gr*) gneisses are possibly isolated from the São Francisco proto-craton by a shallow sea. (b) During the Early Paleoproterozoic, a paleo-coastline is marked by outcrops of the Minas supergroup along the Jeceaba-Bom Sucesso lineament (JBL) to the south and to the east of the São Tiago crust. The first Paleoproterozoic crust was generated in oceanic arcs.

3) A further deformational-metamorphic event was responsible for the gneissic banding S_n transposed in S_{n+1} in the L2 and L3 lithotypes. If such event is correlated with migmatization events described by Toledo et al. (2010; 2667 ± 43 Ma for the neosome), it would be temporary associated with the crystallization of L2, L3 and L4, and be part of the major event of crustal reworking of the southern São Francisco Craton within the 2720–2550 Ma interval (Teixeira et al., 2017). Alternatively, such deformation feature could result from amalgamation of a micro-terrane represented by the São Tiago crust against the São Francisco Proto-craton during Early Paleoproterozoic, and then related to the Mineiro belt.
4) Two new geological units that crop out in the São Tiago region were also identified in this work, the Hbl-bearing tonalitic and granitic gneisses. The Hbl-bearing tonalitic gneiss, of sanukitoid affinity, and the hybrid Hbl-bearing granitic gneiss (2614 ± 13 Ma), whose magmas may be linked to interaction between sanukitoid and crustal-derived melts. The crystallization age of the latter allowed us to bracket the last interval of K-rich magmatism at the southernmost São Francisco Craton from 2614 to 2612 Ma.

The Minas strata along the Jeceaba-Bom Sucesso lineament near the São Tiago region are segmented, encircling the São Tiago Archean crust. Whether this framework represents an original irregular ancient coastline or a micro-terrane amalgamation, and if includes irregular features resulting from dome-and-keel deformational processes are a matter for future research. In any case, our field and geochronological data demonstrate that this lineament is not as simple as previously thought by most authors in terms of the paleogeography of the Mineiro belt and the Archean core of the São Francisco Craton (cf. Campos et al., 2003; Campos and Carneiro, 2008; Neri et al., 2013).

Acknowledgements

M.B. Simon acknowledges Érica Tonetto and Margareth Navarro (UNICAMP) and Débora Nascimento (UFRJ) for their support during laboratory procedures. The senior author also acknowledges F. Farina, O. Laurent and anonymous reviewers of Precambrian Research for their critical and constructive reviews, and Coordenação de Aperfeiçoamento de Pessoal de Nível Superior – CAPES for MSc scholarship grant. This work was partially funded by FAPESP thematic project "*Evolution of Archaean Terranes of the São Francisco Craton and the Borborema Province, Brazil: global environmental and geodynamic implications*" (grant 12/15824-6 awarded to EPO).

Appendix A. Supplementary data

Supplementary data associated with this article can be found, in the online version, at https://doi.org/10.1016/j.precamres.2018.06.015.

References

Aguilar, C., Alkmim, F.F., Lana, C., Farina, F., 2017. Palaeoproterozoic assembly of the São Francisco craton, SE Brazil: new insights from U-Pb titanite and monazite dating. Precambr. Res. 289, 95–115.
Albert, C., Farina, F., Lana, C., Stevens, G., Storey, C., Gerdes, A., Martínez Dopico, C., 2016. Archean crustal evolution in the Southern São Francisco craton, Brazil: constraints from U-Pb, Lu-Hf and O isotope analyses. Lithos 266–267, 64–86.
Alkmim, F.F., Teixeira, W., 2017. The Paleoproterozoic Mineiro belt and the Quadrilátero Ferrífero. In: Heilbron, M., Cordani, U., Alkmim, F. (Eds.), São Francisco Craton, Eastern Brazil: Tectonic Genealogy of a Miniature Continent. Springer International Publishing, Regional Geology Reviews, pp. 71–94.
Alkmim, F.F., Marshak, S., 1998. Transamazonian orogeny in the Southern São Francisco Craton Region, Minas Gerais Brazil: Evidence for a Paleoproterozoic collision and collapse in Quadrilátero Ferrífero. Precambr. Res. 90, 29–58.

Almeida, J.A.C., Dall'Agnol, R., Leite, A.A.S., 2013. Geochemistry and zircon geochronology of the Archean granite suites of the Rio Maria granite-greenstone terrane, Carajás Province, Brazil. J. S. Am. Earth Sci. 42, 103–126.
Alonso-Perez, R., Muntener, O., Ulmer, P., 2009. Igneous garnet and amphibole fractionation in the roots of island arcs: experimental constraints on andesitic liquids. Contrib. Miner. Petrol. 157, 541–558.
Anhaeusser, C.R., Mason, P., Viljoen, M.J., Viljoen, R.P., 1969. A reappraisal of some aspects of precambrian shield geology. Geol. Soc. Am. Bull. 80, 2175–2200.
Arth, J.G., Barker, F., Peterman, Z.E., Frideman, I., 1978. Geochemistry of the gabbro–diorite–tonalite–trondhjemite suite of south-west Finland and its implications for the origin of tonalitic and trondhjemitic magmas. J. Petrol. 19, 289–316.
Ávila, C.A., Teixeira, W., Bongiolo, E.M., Dussin, I.A., Vieira, T.A.T., 2014. Rhyacian evolution of subvolcanic and metasedimentary rocks of the southern segment of the Mineiro belt, São Francisco craton, Brazil. Precambr. Res. 243, 221–251.
Ávila, C.A., Teixeira, W., Cordani, U.G., Moura, C.A.V., Pereira, R.M., 2010. Rhyacian (2.23–2.20 Ga) juvenile accretion in the southern São Francisco craton, Brazil: geochemical and isotopic evidence from the Serrinha magmatic suite, Mineiro belt. J. S. Am. Earth Sci. 29, 464–482.
Baltazar, O.F., Silva, S.L., 1996. Projeto Rio das Velhas: Mapa Geológico Integrado do Supergrupo Rio das Velhas, escala 1:100.000. Departamento Nacional de Produção Mineral/CPRM–Serviço Geológico do Brasil, Belo Horizonte.
Baltazar, O.F., Zucchetti, M., 2000. Rio das Velhas greenstone belt structural evolution, Quadrilátero Ferrífero, Minas Gerais, Brazil. In: International Geological Congress 31, Rio de Janeiro, Brazil. Abstracts, CD-ROM.
Baltazar, O.F., Zucchetti, M., 2007. Lithofacies associations and structural evolution of the Archean Rio das Velhas greenstone belt, Quadrilátero Ferrífero, Brazil: a review of the regional setting of gold deposits. Ore Geol. Rev. 32, 471–499.
Barbosa, N.S., Teixeira, W., Ávila, C.A., Montecino, P.M., Bongiolo, E.M., 2015. 2.17-2.10 Ga plutonic episodes in the Mineiro belt, São Francisco Craton, Brazil: U-Pb ages, geochemical constraints and tectonics. Precambr. Res. 270, 204–225.
Barker, F., 1979. Trondhjemites: definition, environment and hypothesis of origin. In: Barker, F. (Ed.), Trondhjemites, Dacites and Related Rocks. Elsevier, Amsterdam, pp. 1–12.
Barker, F., Arth, J.G., 1976. Generation of trondhjemite–tonalite liquids and Archaean bimodal trondhjemite–basalt suites. Geology 4, 596–600.
Beard, J.S., Lofgren, G.E., 1991. Dehydration melting and water-saturated melting of basaltic and andesitic greenstones and amphibolites at 1, 3, and 6.9 kbar. J. Petrol. 32, 365–401.
Boynton, W.V., 1984. Cosmochemistry of the rare earth element: meteorite studies. In: Henderson, P. (Ed.), Rare Earth Element Geochemistry. Elsevier, Amsterdam, pp. 63–114.
Breaks, F.W., Moore, J.M., 1992. The Ghost Lake batholith, Superior Province of Northwestern Ontario: a fertile, S-type, peraluminous granite – rare-element pegmatite system. Can. Mineral. 30, 835–875.
Brueckner, H.K., Cunningham, D., Alkmim, F.F., Marshak, S., 2000. Tectonic implications of Precambrian Sm–Nd dates from the southern São Francisco craton and adjacent Araçuaí and Ribeira belts, Brazil. Precambr. Res. 99, 255–269.
Campos, J.C.S., Carneiro, M.A., 2008. Neoarchean and Paleoproterozoic granitoids marginal to the Jeceaba-Bom Sucesso lineament (SE border of the southern São Francisco craton): Genesis and tectonic evolution. J. S. Am. Earth Sci. 26, 463–484.
Campos, J.C.S., Carneiro, M.A., Basei, M.A.S., 2003. U-Pb evidence for Neoarchean crustal reworking in southern São Francisco Craton (Minas Gerais, Brazil). Anais da Academia Brasileira de Ciências 75, 497–511.
Campos Neto, M.C., Basei, M.A.S., Janasi, V.A., Moraes, R., 2011. Orogen migration and tectonic setting of the Andrelandia Nappe system: an Ediacaran western Gondwana collage, south of Sao Francisco craton. J. S. Am. Earth Sci. 32 (4), 393–406.
Carneiro, M.A., Endo, I., Nalini Jr., H.A., Sales, J.C.C., Goulart, L.E.A., Silva, E.F., Pereira, A.A., Tavares, T.D., Jiamelaro, F., Carneiro, J.M., Mariano, L.C., Prado, G.E.A., Urbano, E.P.C., Santos, C., Miguel, F.P., 2007. Folha Oliveira escala: 1:100.000: texto explicativo e mapa impresso. Belo Horizonte, CPRM (Brazilian Geological Survey)/UFOP (Federal University of Ouro Preto) Partnership 127, p.
Carneiro, M.A., Teixeira, W., Carvalho Jr, I.M., Fernandes, R.A., 1998. Ensialic tectonic setting of the Archaean Rio das Velhas greenstone belt: Nd and Pb isotopic evidence from the Bonfim metamorphic complex, Quadrilátero Ferrífero, Brazil. Revista Brasileira de Geociências 28, 189–200.
Champion, D.C., Sheraton, J.W., 1997. Geochemistry and Nd isotope systematics of Archaean granites of the Eastern Goldfields, Yilgarn Craton, Australia: implications for crustal growth processes. Precambr. Res. 83 (1–3), 109–132.
Chemale Jr., F., Rosière, C.A., Endo, I., 1994. The tectonic evolution of the Quadrilátero Ferrífero, Minas Gerais, Brazil. Precambr. Res. 65, 25–54.
Condie, K.C., 2005. TTGs and adakites: are they both slab melts? Lithos 80, 33–44.
Condie, K.C., Hunter, D.R., 1976. Trace element geochemistry of Archaean granitic rocks from Barberton region, South Africa. Earth Planet. Sci. Lett. 29, 389–400.
CPRM (Brazilian Geological Survey)/Codemig (Companhia de Desenvolvimento Econômico do Estado de Minas Gerais) Partnership, 2014. Geological Map of the State of Minas Gerais. Programa Geologia do Brasil, Integração, Atualização e Difusão de Dados da Geologia do Brasil - Projeto Mapas Geológicos Estaduais.
Dickinson, W., Gehrels, G., 2003. U-Pb ages of detrital zircons from Permian and Jurassic eolian sandstones of the Colorado Plateau, USA: paleogeographic implications. Sed. Geol. 163, 29–66.
Dorr II, J.V., 1969. Physiographic, stratigraphic and structural development of the Quadrilátero Ferrífero, Minas Gerais Brazil. US Geol. Survey Profess. Paper 614-A, 110 p.
Ellam, R.M., Hawkesworth, C.J., 1988. Is average continental crust generated at subduction zones? Geology 16, 314–317.
Engler, A., Koller, F., Meisel, T., Quéméneur, J., 2002. Evolution of the Archean/Proterozoic crust in the southern São Francisco craton near Perdões, Minas Gerais, Brazil: petrological and geochemical constraints. J. S. Am. Earth Sci. 15, 709–723.
Farina, F., Albert, C., Lana, C., 2015. The Neoarchean transition between medium and high-K granitoids: clues from the Southern São Francisco Craton (Brazil). Precambr. Res. 266, 375–394.
Farina, F., Albert, C., Martínez Dopico, C., Aguilar Gil, C., Moreira, H., Hippertt, J.P., Cutts, K., Alkmim, F.F., Lana, C., 2016. The Archean-Paleoproterozoic evolution of the Quadrilatero Ferrífero (Brasil): current models and open questions. J. S. Am. Earth Sci. 68, 4–21.
Feng, R., Kerrich, R., 1992. Geochemical evolution of granitoids from the Archean Abitibi Southern Volcanic Zone and the Pontiac subprovince, Superior Province, Canada: implications for tectonic history and source regions. Chem. Geol. 98, 23–70.
Frost, C.D., Frost, B.R., Kirkwood, R., Chamberlain, K.R., 2006. The tonalite–trondhjemite–granodiorite (TTG) to granodiorite–granite (GG) transition in the late Archean plutonic rocks of the central Wyoming Province. Can. J. Earth Sci. 43, 1419–1444.
Goulart, L.E.A., Carneiro, M.A., Endo, I., Suita, M.T.F., 2013. New evidence of Neoarchean crustal growth in southern São Francisco Craton: the Carmópolis de Minas Layered Suite, Minas Gerais Brazil. Brazilian J. Geol. 43 (3), 445–459.
Hartmann, L.A., Endo, I., Suita, M.D.F., Santos, J.O.S., Frantz, J.C., Carneiro, M.A., McNaughton, N.J., Barley, M.E., 2006. Provenance and age delimitation of Quadrilátero Ferrífero sandstones based on zircon U-Pb isotopes. J. S. Am. Earth Sci. 20, 273–285.
Heilimo, E., Halla, J., Hölttä, P., 2010. Discrimination and origin of the sanukitoid series: geochemical constraints from the Neoarchean western Karelian Province (Finland). Lithos 115, 27–39.
Heimlich, R.A., Banks, P.O., 1968. Radiometric age determinations, Bighorn Mountains, Wyoming. Am. J. Sci. 266, 180–192.
Jayananda, M., Chardon, D., Peucat, J.-J., Capdevila, R., 2006. 2.61 Ga potassic granites and crustal reworking in the western Dharwar craton, southern India: tectonic, geochronologic and geochemical constraints. Precambr. Res. 150 (1–2), 1–26.
Jordt-Evangelista, H., Alkmim, F.F., Marshak, S., 1992. Metamorfismo Progressivo e a Ocorrência de três polimorfos de Al_2SiO_5 (cianita, andaluzita, silimanita) na Formação Sabará em Ibirité, Quadrilátero Ferrífero, MG. Revista da Escola de Minas 45, 157–160.
Kent, R.W., Hardarson, B.S., Saunders, A.D., Storey, M., 1996. Plateaux ancient and modern: geochemical and sedimentological perspectives on Archaean oceanic magmatism. Lithos 37, 129–142.
Koglin, N., Zeh, A., Cabral, A.R., Gomes, A.V.C., Neto, A.V.C., Brunetto, W.J., Galbi-atti, H., et al., 2014. Depositional age and sediment source of the auriferous Moeda Formation, Quadrilátero Ferrífero of Minas Gerais Brazil: new constraints from U-Pb–Hf isotopes in zircon and xenotime. Precambr. Res. 255, 96–108.
Lana, C., Alkmim, F.F., Armonstrong, R., Scholz, R., Romano, R., Nalini Jr., H.R., 2013. The ancestry and magmatic evolution of Archaean TTG rocks of the Quadrilátero Ferrífero province, Southeast Brazil. Precambr. Res. 231, 157–173.
Laurent, O., Martin, H., Moyen, J.F., Doucelance, R., 2014. The diversity and evolution of late-Archean granitoids: evidence for the onset of "modern-style" plate tectonics between 3.0 and 2.5 Ga. Lithos 205, 208–235.
Machado, N., Carneiro, M.A., 1992. U-Pb evidence of Late Archean tectonothermal activity in southern São Francisco shield, Brazil. Can. J. Earth Sci. 29, 2341–2346.
Machado, N., Noce, C.M., Ladeira, E.A., de Oliveira, O.A.B., 1992. U-Pb geochronology of the Archean magmatism and Proterozoic metamorphism in the Quadrilátero Ferrífero, southern São Francisco Craton, Brazil. Geol. Soc. Am. Bull. 104, 1221–1227.
Machado, N., Schrank, A., Noce, C.M., Gauthier, G., 1996. Ages of detrital zircon from Archean-Paleoproterozoic sequences: implications for Greenstone Belt setting evolution of a Transamazonian foreland basin in Quadrilátero Ferrífero, southeast Brazil. Earth Planet. Sci. Lett. 141, 259–276.
Marshak, S., Alkmim, F.F., Jordt-Evangelista, H., 1992. Proterozoic crustal extension and the generation of dome-and-keel structures in an Archaean granite–greenstone terrane. Nature 357, 491–493.
Marshak, S., Tinkham, D., Alkmim, F.F., Brueckner, H., Bornhorst, T., 1997. Dome-and-keel provinces formed during Paleoproterozoic orogenic collapse: Diapir clusters or core complexes? Examples from the Quadrilátero Ferrífero (Brazil) and the Penokean Orogen (USA). Geology 25, 415–418.
Martin, H., 1986. Effect of steeper Archean geothermal gradient on geochemistry of subduction-zone magmas. Geology 14, 753–756.
Martin, H., Moyen, J.F., Guitreau, M., Blichert-Toft, J., Le Pennec, J.L., 2014. Why Archaean TTG cannot be generated by MORB melting in subduction zones. Lithos 198–199, 1–13.
Martin, H., Moyen, J.F., Rapp, R.P., 2009. The sanukitoid series: magmatism at the Archaean-Proterozoic transition. Earth Environ. Sci. Trans. R. Soc. Edinburgh 100 (1–2), 15–33.
Martínez Dopico, C.I., Lana, C., Moreira, H.S., Cassino, L.F., Alkmim, F.F., 2017. U-Pb ages and Hf-isotope data of detrital zircons from the late Neoarchean-Paleoproterozoic Minas Basin, SE Brazil. Precambr. Res. 291, 143–161.
McDonough, W.F., Sun, S.-S., 1995. The composition of the Earth. Chem. Geol. 120, 223–253.
Mendes, M.C.O., Lobato, L.M., Suckau, V., Lana, C., 2014. In situ LA-ICPMS U-Pb dating of detrital zircons from the Cercadinho Formation, Minas Supergroup. Revista Geologia USP. Série Científica 14 (1), 55–68.
Montel, J.M., Vielzeuf, D., 1997. Partial melting of metagreywackes, part II. Compositions of minerals and melts. Contr. Mineral. Petrol. 128, 176–196.
Moreira, H., Lana, C., Nalini Jr., H.A., 2016. The detrital zircon record of an Archaean convergent basin in theSouthern São Francisco Craton, Brazil. Precambr. Res. 275, 84–99.

Moreno, J.A., Baldim, M.R., Semprich, J., Oliveira, E.P., Verma, S.K., Teixeira, W., 2017. Geochronological and geochemical evidences for extension-related Neoarchean granitoids in the southern São Francisco Craton, Brazil. Precambr. Res. 294, 322–343.
Moyen, J.F., 2011. The composite Archaean grey gneisses: petrological significance, and evidence for a non-unique tectonic setting for Archaean crustal growth. Lithos 123, 21–36.
Moyen, J.F., Martin, H., 2012. Forty years of TTG research. Lithos 148, 312–336.
Moyen, J.F., Martin, H., Jayananda, M., Auvray, B., 2003. Late Archaean granites: a typology based on the Dharwar Craton (India). Precambr. Res. 127 (1–3), 103–123.
Nair, R., Chacko, T., 2008. Role of oceanic plateaus in the initiation of subduction and origin of continental crust. Geology 36, 583–586.
Navarro, M.S., Tonetto, E.M., Oliveira, E.P., 2015. LA-SF-ICP-MS U-Pb Zircon Dating at University of Campinas, Brazil. Geonalysis 2015, Vienna, Austria, pp. 09.
Neri, M.E.N.V., Rosière, C.A., Lana, C.C., 2013. Supergrupo Minas na Serra de Bom Sucesso, extremo sudoeste do Quadrilátero Ferrífero – MG: petrografia, geoquímica e isótopos de U-Pb. Revista Geologia USP. Série Científica 13 (2), 117–202.
Noce, C.M., Machado, N., Teixeira, W., 1998. U-Pb geochronology of gneisses and granitoids in the Quadrilátero Ferrífero (Southern São Francisco Craton): age constraints for Archean and Paleoproterozoic magmatism and metamorphism. Revista Brasileira de Geociências 28, 95–102.
Noce, C.M., Teixeira, W., Machado, N., 1997. Geoquímica dos gnaisses TTG e granitoides neoarqueanos do Complexo Belo Horizonte, Quadrilátero Ferrífero. Minas Gerais. Revista Brasileira de Geociências 27 (1), 25–32.
Noce, C.M., Zuccheti, M., Baltazar, O.F., Armstrong, R., Dantas, E., Renger, F.E., Lobato, L.M., 2005. Age of felsic volcanism and the role of ancient continental crust in the evolution of the Neoarchean Rio das Velhas greenstone belt (Quadrilátero Ferrífero, Brazil): U-Pb zircon dating of volcaniclastic graywackes. Precambr. Res. 141, 67–82.
O'Connor, J.T., 1965. A classification for quartz-rich igneous rocks based on feldspar ratios. U.S. Geol. Surv. Prof. Pap. 525 79–84 (B).
Patiño Douce, A.E., 2005. Vapor-absent melting of tonalite at 15–32 kbar. J. Petrol. 46, 275–290.
Patiño Douce, A.E., Beard, J.S., 1995. Dehydration-melting of biotite gneiss and quartz amphibolite from 3 to 15 kbar. J. Petrol. 36, 707–738.
Paton, C., Woodhead, J.D., Hellstrom, J.C., Hergt, J.M., Greig, A., Maas, R., 2010. Improved laser ablation U-Pb zircon geochronology through robust downhole fractionation correction. Geochem. Geophys. Geosyst. 11 (3), Q0AA06.
Peccerillo, A., Taylor, S.R., 1976. Geochemistry of Eocene calc-alkaline volcanic rocks from the Kastamonu area, Northern Turkey. Contr. Mineral. Petrol. 58, 63–81.
Petrus, J.A., Kamber, B.S., 2012. VizualAge: a novel approach to laser ablation ICP-MS U-Pb geochronology data reduction. Geostand. Geoanal. Res. 36, 247–270.
Queménéur, J.J.G., Esboço estratigráfico, estrutural e metamórfico da Serra de Bom Sucesso (MG). In: Simpósio de Geologia de Minas Gerais 4, Belo Horizonte, Brazil. Anais, p. 135–148.
Renger, F.E., Noce, C.M., Romano, A.W., Machado, N., 1994. Evolução sedimentar do Supergrupo Minas: 500 Ma. de registro geológico no Quadrilátero Ferrífero, Minas Gerais, Brasil. Geonomos 2 (1), 1–11.
Romano, R., Lana, C., Alkmim, F.F., Stevens, G.S., Armstrong, R., 2013. Stabilization of the southern portion of the São Francisco Craton, SE Brazil, through a long-lived period of potassic magmatism. Precambr. Res. 224, 143–159.
Seixas, L.A.R., David, J., Stevenson, R., 2012. Geochemistry, Nd isotopes and U-Pb geochronology of a 2350 Ma TTG suite, Minas Gerais, Brazil: implications for the crustal evolution of the southern São Francisco craton. Precambr. Res. 196–197, 61–80.
Shand, S.J., 1943. The eruptive rocks, 2nd edition. John Wiley, New York, pp. 444.
Silva, L.C., Armstrong, R., Noce, C.M., Carneiro, M.A., Pimentel, M., Pedrosa-Soares, A.C., Leite, C.A., Vieira, V.S., Silva, M.A., Paes, V.J.C., Cardoso Filho, J.M., 2002. Reavaliação da evolução geológica em terrenos pré-Cambrianos brasileiros com base em novos dados U-Pb SHRIMP, parte II: Orógeno Araçuaí, Cinturão Mineiro e Cráton São Francisco Meridional. Revista Brasileira de Geociências 32 (4), 513–528.
Smith, T.E., Choudhry, A.G., Huang, C.H., 1983. The geochemistry and petrogenesis of the Archean Gamitagama Lake igneous complex, southern Superior Province. Precambr. Res. 22, 219–244.
Smithies, R.H., 2000. The Archean tonalite–tondhjemite-granodiorite (TTG) series is not an analogue of cenozoic adakite. Earth Planet. Sci. Lett. 182, 115–125.
Streckeisen, A., 1976. To each plutonic rock, its proper name. Earth Sci. Rev. 12 (1), 1–33.
Sylvester, P.J., 1994. Archaean granite plutons. In: Condie, K.C. (Ed.), Archaean Crustal Evolution. Developments in Precambrian Geology 11. Elsevier, Amsterdam, pp. 261–314.
Teixeira, W., Ávila, C.A., Dussin, I.A., Corrêa Neto, A.V., Bongiolo, E.M., Santos, J.O., Barbosa, N.S., 2015. A juvenile accretion episode (2.35–2.32 Ga) in the Mineiro belt and its role to the Minas accretionary orogeny: Zircon U-Pb–Hf and geochemical evidences. Precambr. Res. 256, 148–169.
Teixeira, W., Cordani, U.G., Nutman, A.P., Sato, K., 1998. Polyphase Archean evolution in the Campo Belo metamorphic complex, Southern São Francisco Craton, Brazil: SHRIMP U-Pb zircon evidence. J. S. Am. Earth Sci. 11 (3), 279–289.
Teixeira, W., Oliveira, E.P., Marques, L.S., 2017. Nature and Evolution of the Archean Crust of the São Francisco Craton. In: Heilbron, M., Cordani, U., Alkmim, F. (Eds.), São Francisco Craton, Eastern Brazil; Tectonic Genealogy of a Miniature Continent. Regional Geology Reviews. Springer International Publishing, pp. 29–56.
Toledo, C.L.B., Silva, A.M., Hackspacher, P.C., Beghelli Jr., L.P., 2010. Novas evidências para a arquitetura de domos e quilhas na borda meridional do cráton São Francisco. Congresso Brasileiro de Geologia 45, Belém, Brazil. Anais, pp. 91.
Trouw, R.A.J., Peternel, R., Ribeiro, A., Heilbron, M., Vinagre, R., Duffles, P., Trouw, C.C., Fontainha, M., Kussama, H.H., 2013. A new interpretation for the interference zone between the southern Brasília belt and the central Ribeira belt, SE Brazil. J. S. Am. Earth Sci. 48, 43–57.
Vendemiatto, M.A., Enzweiler, J., 2001. Routine control of accuracy in silicate rock analysis by X-ray fluorescence spectrometry. Geostandards Newslett.: J. Geostandards Geoanal. 25, 283–291.
Verma, S.K., Verma, S.P., Oliveira, E.P., Singh, V.K., Moreno, J.A., 2016. LA-SF-ICP-MS zircon U-Pb geochronology of granitic rocks from the central Bundelkhand greenstone complex, Bundelkhand craton, India. J. Asian Earth Sci. 118, 125–137.
Whalen, J.B., Percival, J.A., McNicoll, V.J., Longstaffe, F.J., 2004. Geochemical and isotopic (Nd–O) evidence bearing on the origin of late- to post-orogenic high-K granitoid rocks in the western Superior Province: implications for late-Archaean tectonomagmatic processes. Precambr. Res. 132, 303–326.
Watkins, J.M., Clemens, J.D., Treloar, P.J., 2007. Archaean TTGs as sources of younger granitic magmas: melting of sodic metatonalites at 0.6–1.2 GPa. Contributions to Mineralogy and Petrology 154, 91–110.Whitney, D.L., Evans, B.W., 2010. Abbreviations for names of rock-forming minerals. Am. Mineral. 95, 185–187.
Wiedenbeck, M., Allé, P., Corfu, F., Griffin, W.L., Meier, M., Oberli, F., von Quadt, A., Roddick, J.C., Spiegel, W., 1995. Three natural zircon standards for U-Th–Pb, Lu–Hf, trace element and REE analyses. Geostandards Newslett. 19, 1–23.
Windley, B.F., 1995. The Evolving Continents. Chester, John Wiley and sons, pp. 526.
Zucchetti, M., Baltazar, O.F., Raposo, F.O., 1998. Estratigrafia. In: M. Zucchetti, O.F. Baltazar (Eds.), Projeto Rio das Velhas – Texto explicativo do mapa geológico integrado, escala 1:100.000. 2nd ed. Departamento Nacional de Produção Mineral/CPRM–Serviço Geológico do Brasil, Belo Horizonte, pp. 13–42.